Toxicology and Applied Pharmacology 409 (2020) 115284

Contents lists available at ScienceDirect

Toxicology and Applied Pharmacology

journal homepage: www.elsevier.com/locate/taap

Biological effects of inhaled hydraulic fracturing sand dust. IV. Pulmonary effects

Kristen A. Russ [a], Janet A. Thompson [a], Jeffrey S. Reynolds [a], Robert R. Mercer [a], Dale W. Porter [a], Walter McKinney [a], Richard D. Dey [b,c], Mark Barger [a], Jared Cumpston [a], Thomas P. Batchelor [b,c], Michael L. Kashon [a], Vamsi Kodali [a], Mark C. Jackson [a], Krishnan Sriram [a], Jeffrey S. Fedan [a,*]

[a] Health Effects Laboratory Division, National Institute for Occupational Safety and Health, Morgantown, WV 26505, United States of America
[b] Department of Physiology and Pharmacology, Anatomy and Laboratory Medicine, Robert C. Byrd Health Sciences Center, West Virginia University, Morgantown, WV 26506, United States of America
[c] Department of Pathology, Anatomy and Laboratory Medicine, Robert C. Byrd Health Sciences Center, West Virginia University, Morgantown, WV 26506, United States of America

ARTICLE INFO

Keywords:
Hydraulic fracturing
Fracking sand dust
Lung
Pulmonary toxicity

ABSTRACT

Hydraulic fracturing creates fissures in subterranean rock to increase the flow and retrieval of natural gas. Sand ("proppant") in fracking fluid injected into the well bore maintains fissure patency. Fracking sand dust (FSD) is generated during manipulation of sand to prepare the fracking fluid. Containing respirable crystalline silica, FSD could pose hazards similar to those found in work sites where silica inhalation induces lung disease such as silicosis. This study was performed to evaluate the possible toxic effects following inhalation of a FSD (FSD 8) in the lung and airways. Rats were exposed (6 h/d × 4 d) to 10 or 30 mg/m^3 of a FSD collected at a gas well, and measurements were performed 1, 7, 27 and, in one series of experiments, 90 d post-exposure. The following ventilatory and non-ventilatory parameters were measured *in vivo* and/or *in vitro*: 1) lung mechanics (respiratory system resistance and elastance, tissue damping, tissue elastance, Newtonian resistance and hysteresivity); 2) airway reactivity to inhaled methacholine (MCh); airway epithelium integrity (isolated, perfused trachea); airway efferent motor nerve activity (electric field stimulation *in vitro*); airway smooth muscle contractility; ion transport in intact and cultured epithelium; airway effector and sensory nerves; tracheal particle deposition; and neurogenic inflammation/vascular permeability. FSD 8 was without large effect on most parameters, and was not pro-inflammatory, as judged histologically and in cultured epithelial cells, but increased reactivity to inhaled MCh at some post-exposure time points and affected Na^+ transport in airway epithelial cells.

1. Introduction

This is the fourth in a series of tandem papers in which the potential toxicity of fracking sand dust (FSD) in several organ systems has been investigated. Its focus is on an examination of the effects of inhalation exposure to one FSD, *i.e.*, FSD 8, collected at hydraulic fracturing sites, on ventilatory and non-ventilatory function of the lung and airways of rats. The chemical properties and particle characteristics of nine FSDs and MIN-U-SIL® 5 (MIN-U-SIL), and their effects following intratracheal (i.t.) instillation in rats, were described in the preceding paper of this series (Fedan et al., 2020). The first paper in the series (Fedan, 2020) describes the overall approach to the investigation in the context of current knowledge about silica toxicity and research gaps. In the second paper (Fedan et al., 2020), FSD 8 particle characteristics and the effects of intratracheal (i.t.) instillation on the development of lung inflammation was investigated. The other studies in this series have examined the effects of FSD 8 on the cardiovascular, immune and nervous systems, brain and kidney (Anderson et al., 2020; Sager et al., 2020; Krajnak et al., 2020; Sriram et al., 2020), as well as cytotoxicity (Olgun et al., 2020), and the results have been summarized (Investigative Team, 2020).

Fracking sand dust contains crystalline silica. Disabling and

* Corresponding authors at: Pathology and Physiology Research Branch, National Institute for Occupational Safety and Health, 1000 Frederick Lane, Morgantown, WV 26508, United States of America.
E-mail address: jsf2@cdc.gov (J.S. Fedan).

https://doi.org/10.1016/j.taap.2020.115284
Received 17 July 2020; Received in revised form 7 October 2020; Accepted 10 October 2020
Available online 15 October 2020
0041-008X/Published by Elsevier Inc.

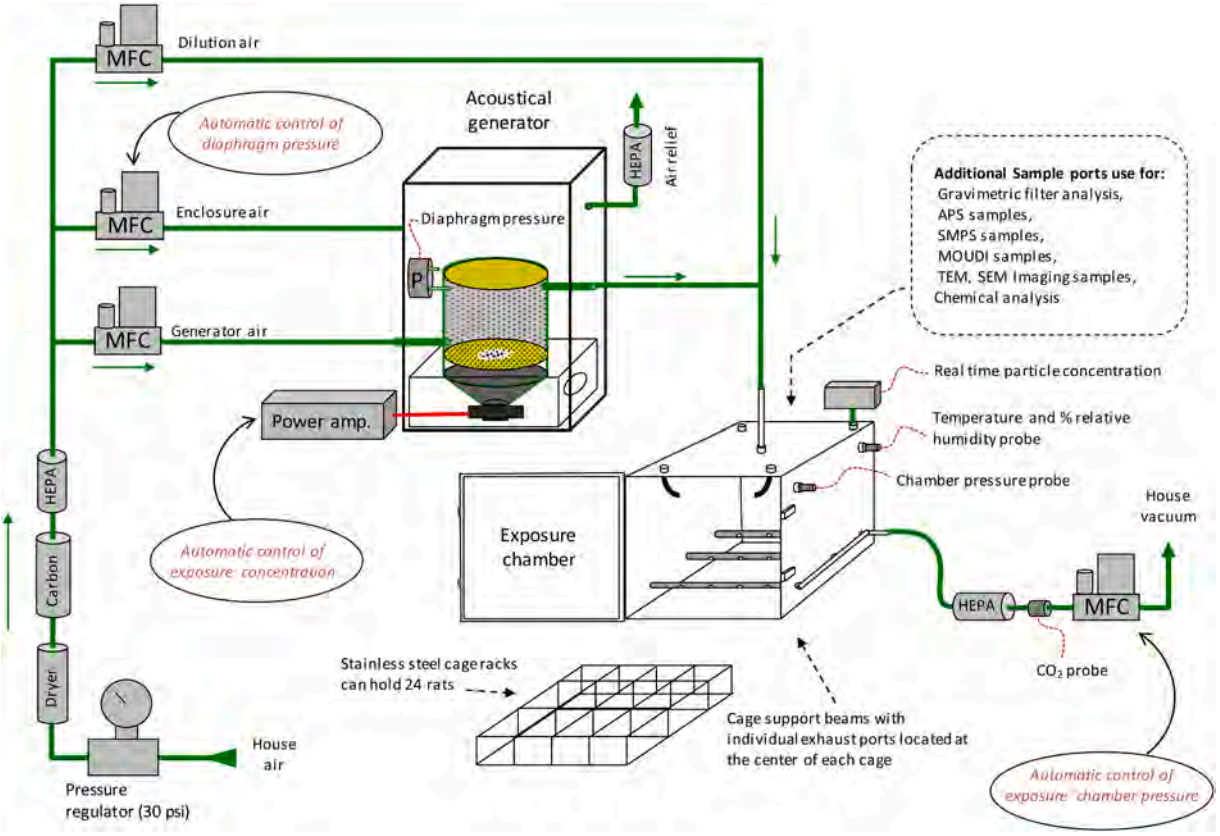

Fig. 1. Schematic diagram of the FSD inhalation exposure system. Abbreviations: MFC, mass flow controller; APS, aerosol particle sizer; SMPS, scanning mobility particle sizer; MOUDI, microorifice uniform deposit impactor; TEM, transmission electron microscope; SEM, scanning electron microscope.

potentially fatal lung diseases, including silicosis and lung cancer, can be caused by chronic exposure to crystalline silica and many different types of dusts that contain crystalline silica (Hubbs et al., 2005; Kuempel et al., 2001; National Institute for Occupational Safety and Health, 2002). However, existing published reports on silica's effects in the lung have not considered broadly the evaluation of pulmonary functional changes that may occur prior to the development of lung cancer or chronic silicosis. These changes may potentially occur at lower lung burdens and shorter latency than silicosis and lung cancer. Therefore, the purpose of the present study was to examine the effects of inhaled FSD 8 on several ventilatory and non-ventilatory functions of the lung and airways, using a rat model. Pulmonary mechanics was assessed to ascertain whether breathing could be adversely affected by FSD 8. Airway reactivity to inhaled methacholine (MCh) was measured because airway hyperreactivity is associated with a variety of lung diseases, such as asthma and chronic obstructive pulmonary disease. Reactivity of airway smooth muscle to MCh *in vitro*, and the integrity of the airway epithelium in controlling reactivity, were examined in the isolated, perfused trachea. Efferent motor nerve activity is important in regulating airway diameter; thus, responses of airway smooth muscle to electrically-stimulated neurotransmitter release were studied in isolated airway smooth muscle preparations. Likewise, the release of neuropeptides from sensory nerves in airways, which is a component of neurogenic inflammation and which increases vascular permeability, was assessed using the Evans blue dye method. Maintenance of the airway surface liquid is critical to the efficient removal of particles from the lung *via* the mucociliary escalator, and airway surface composition and height are regulated by epithelial ion transport; thus, ion transport was examined in this study. To our knowledge, these investigations have not previously been conducted.

The results of this investigation suggest that short-term inhalation exposure to FSD 8 had little effect on most ventilatory and non-ventilatory lung functions; however, reactivity to inhaled MCh was increased modestly, and tracheal epithelial Na^+ transport was inhibited, by exposure to FSD 8.

2. Methods

2.1. Animals

All studies were conducted in facilities accredited by AAALAC International, were approved by the Institutional Animal Care and Use Committee and were in compliance with the Public Health Service Policy on Humane Care and Use of Laboratory Animals and the NIH Guide for the Care and Use of Laboratory Animals. Male Sprague-Dawley rats [H1a: (SD) CVF], approximate body weight of 200–225 g at arrival, were obtained from Hilltop Lab Animals, Inc. (Scottdale, PA). All animals were free of viral pathogens, parasites, mycoplasm, *Helicobacter* and cilia-associated respiratory bacillus. Animals were acclimated for 1 wk and housed in pairs in ventilated micro-isolator units supplied with HEPA-filtered laminar flow air (Thoren Caging Systems; Hazleton, PA), with Harlan 7090C Sani Chip and 7070 Diamond Dry combination for bedding, and provided tap water and Harlan 2918 irradiated Teklad Global 18% rodent chow *ad libitum*. Rats were housed under controlled light cycle (12 h light/12 h dark) and temperature (22–25 °C) conditions.

In all *in vitro* experiments rats were given an overdose of sodium pentobarbital-based euthanasia solution (100–300 mg/kg, i.p.; Vortec Pharmaceuticals LTD) and euthanized by exsanguination, or were anesthetized and euthanized post-procedure.

2.2. FSD 8 inhalation exposures

FSD 8, one of nine FSDs collected from domestic drilling sites where fracking was employed (Fedan et al., 2020), was used in this study. Rats

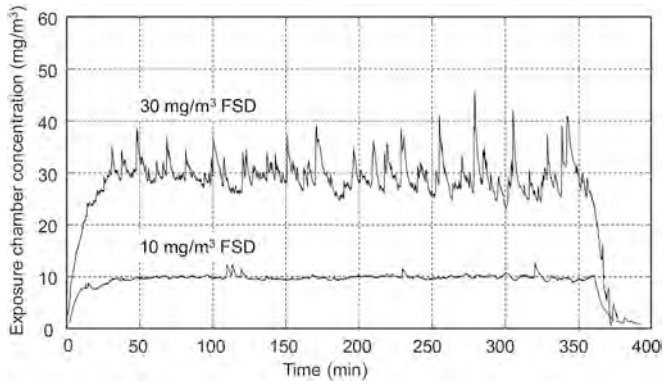

Fig. 2. FSD 8 mass concentrations in the exposure chamber during generation of 10 and 30 mg/m^3 aerosols. (FSD 8 is abbreviated as FSD in the figures.) After reaching 95% of the desired concentrations the levels of FSD were constant over the 6-h period used for exposing animals.

which had been acclimated to the facility for at least a week were exposed by whole body inhalation using an acoustical particle generator system (Fig. 1; McKinney et al., 2012) with the following modifications: generator flow was increased to 10 l/min and venturi/dilution air flow was increased to 40 l/min. The increase in airflow was necessary to accommodate a larger exposure chamber that could hold twenty-four rats at a time. Slight modifications were also made to the custom control software to optimize the feedback control systems for the larger chamber.

Animals were exposed to FSD 8 aerosol for 6 h/d for four consecutive d at either 10 or 30 mg/m^3. The two doses of FSD 8 aerosol used for the exposures were chosen to model the effects of typical exposures of workers (see *2.3.*). Fig. 2 illustrates that the aerosol levels were constant over this 6-h period. As well, particle concentrations inside the exposure chamber were verified daily by gravimetric analysis. Control animals, placed in separate chambers, identical in design and functionality, breathed filtered air for the same periods and were otherwise handled identically. During inhalation exposures, the animals did not have access to food or water. In previous investigations involving exposures to other agents, animals manipulated in such a manner have not exhibited any observable body weight changes, or behavioral or adverse toxicological effects due to food/water deprivation. The exposure chamber contained ~300 l and was approximately 24″ × 24″ × 50″. Stainless steel cages made of ½" × ½" mesh, and 5″ × 5″ × 6.7″ (H × W × L) in dimensions, housed the animals. Individual cages were on two planes. Airflow through the chamber was maintained at 50 l/min (12 air changes/h); chamber air temperature was 70–74 °F; chamber air relative humidity was 30–65%; chamber pressure was 0″ of H_2O. Levels were monitored in real time and gave CO_2: ≤ 5000 ppm and ammonia: ≤ 25 ppm.

Experimental end points for all organ system studies were examined at 1, 7 and 27 d post-exposure and, in one series of experiments, a 90 d post-exposure point was used to assess lung inflammatory changes.

potential exposure concentration and exposure duration that this study modeled (see also Hubbs et al., 2005). The calculations made here do not account for clearance or the influence of other human confounding factors but provides a plausible estimate of the worker deposition burden that our experimental paradigm mimics. The calculations were made with the following assumptions:

The MMAD for FSD 8 aerosol was determined to be 1.75 μm (see Fig. 6) indicating that it is largely in the fine particle range, although small amounts of ultrafine-sized particles were also observed. At this particle size, the deposition efficiency is predicted to be around 11–15% (Raabe et al., 1988; MPPD, 2010). To estimate the total lung deposition in the rat [$LB_{(rat)}$] following low or high dose FSD 8 exposure, the following equation was used,

$$LB_{(rat)} = AC_{FSD\ 8} \times MV_{(rat)} \times ED \times DE.$$

By taking into account the aerosol concentration ($AC_{FSD\ 8}$; 10 or 30 mg/m^3), rat minute ventilation volume [$MV_{(rat;\ 300g\ body\ weight)}$; 0.21 × 10^{-3} m^3/min; MPPD, 2010], exposure duration (ED; 6 h/d × 4d × 60 min/h) and a deposition efficiency (DE) for fine particles of 13% (median of the 11–15% reported value, as above), the $LB_{(rat)}$ following a low or high dose FSD 8 exposure was estimated to be 0.392 mg and 1.18 mg, respectively.

Next, to relate the rat dosing paradigm employed in this study to workplace exposures, the equivalent FSD 8 lung burden in humans was determined using surface area of alveolar epithelium (rat = 0.4 m^2; human = 102 m^2) as a dose metric (Stone et al., 1992). From this, the FSD 8 lung burden in a human worker after a low or high dose exposure was estimated to be 99.96 (~100 mg) and 300.9 (~300 mg), respectively.

The NIOSH recommended exposure limit (REL) for crystalline silica (quartz) is 0.05 mg/m^3 TWA (time-weighted average). Likewise, OSHA permissible exposure limit (PEL) is 0.05 mg/m^3 averaged over an 8-h day. However, aerosol measurements at fracking well sites have shown that the levels of respirable crystalline silica often exceed the occupational exposure limits, sometimes by over 10-fold (Esswein et al., 2013). If worker exposure occurred at this 10-fold higher rate of 0.5 mg/m^3, the number of days of exposure required to achieve a FSD 8 lung deposition of 100 mg and 300 mg in a worker can be estimated using the following formula,

$$\text{Days of exposure} = LB_{(human\ worker)} \big/ \left[AC_{Si} \times MV_{(worker)} \times ED \times DE\right]$$

where, AC_{Si} is the aerosol concentration of crystalline silica (quartz; 10-fold the NIOSH REL = 0.5 mg/m^3), $LB_{(human\ worker)}$ is the predicted lung burden in a human worker (100 mg or 300 mg; as calculated above), $MV_{(worker)}$ is the minute ventilation rate for a reference worker (a human performing moderate-heavy exercise; 20 × 10^{-3} m^3/min; ICRP, 1994), ED is the exposure duration assuming a 8 h work schedule (8 h/d × 60 min/h) and DE is the deposition efficiency of particles in the pulmonary alveoli (predicted as 13% based on MMAD of fine particles; Raabe et al., 1988; ICRP, 1994; MPPD, 2010). Incorporating the above values in the formula,

$$\begin{aligned}\text{Days of exposure} &= 100 \text{ or } 300 \text{ mg} \big/ \left[(0.5 \text{ mg/m}^3) \times (20 \times 10^{-3} \text{ m}^3/\text{min}) \times (8 \text{ h/d} \times 60 \text{ min/h}) \times 0.13\right] \\ &= 100 \text{ or } 300 \text{ mg} / [0.624] \\ &= \sim 160 \text{ or } 481 \text{ d}\end{aligned}$$

2.3. Relevance of animal inhalation dosing paradigm to potential workplace exposures

To relate the animal inhalation exposure to worker exposure conditions, mathematical calculations were utilized to determine the

Assuming a 240-d work year, the number of years of exposure required to achieve an FSD 8 lung burden of 100 mg is about 0.66 y and that for 300 mg is about 2 y. Thus, our 4-d inhalation exposure to the low

(10 mg/m^3) or high (30 mg/m^3) dose FSD 8 in the rodent model mimics a FSD 8 exposure paradigm of ~0.66 or 2 y in a worker, respectively, when exposure occurs at a concentration that is 10-fold higher than the occupational exposure limits (NIOSH REL or OSHA PEL) for crystalline silica.

2.4. FSD 8 particle aerodynamic mass distribution and particle count size distribution

The particle aerodynamic mass distribution of the respirable FSD 8 aerosol inside the exposure chamber was determined using a 10-stage impactor (MOUDI, model 110-R; Applied Physics, Inc.; Monte Vista, CO) in series with a nano-impactor (MOUDI, model 115). Particle count size distribution of the FSD 8 aerosol inside the exposure chamber was determined with a Scanning Mobility Particle Sizer (SMPS; model 3034; TSI Inc., Shoreview, MN).

2.5. Lung weights

To assess whether lung edema developed following FSD 8 inhalation, after euthanasia the lungs were removed from rats, weighed to obtain wet weight, freeze-dried, and weighed again to obtain dry weight.

2.6. Dark-field microscopic analysis of FSD 8 lung clearance

The retention/clearance of FSD 8 particles in the lung after a single inhalation exposure to 30 mg/m^3 FSD 8 (6 h) was assessed. One, 7, 27 and 90 d after inhalation rats were euthanized and the lungs were removed, sectioned and stained with sirius red and hematoxylin.

FSD 8 particles in the sections were assessed using dark-field microscopy. This method of imaging is used to scan lung sections at relatively low magnification to identify particles that would not be detected by another microscopy means (McKinney et al., 2012; Mercer et al., 2013, 2018; Ma et al., 2015). Typically, the image intensity of particles in tissue sections is approximately 20-fold that of the embedded tissue (Mercer et al., 2018).

Sections for dark-field examination were cut from paraffin blocks at 5 μ thickness and collected on silica dust-free, ultrasonically cleaned, laser cut slides (Schott North America Inc.; Duryea, PA) to avoid silica contamination from the ground edges of traditional slides. After staining with sirius red-hematoxylin, slides were dehydrated in xylene and coverslipped with Permount (Fisher Scientific Co.; Pittsburgh, PA) containing 5% by volume xylene. Just before mounting, the xylene-Permount was centrifuged at 10,000×g × 10 min to remove contaminating particles in the Permount.

The optical microscopes consist of a transmitted light microscope (Olympus B63 with motorized condenser, controller and reflected light system) and a CytoViva EDM (CytoViva; Auburn, AL). The CytoViva EDM has a high signal-to-noise, dark-field illumination optical system adapted to an Olympus BX41 microscope, which also includes a hyperspectral imaging camera with ENVI 4.8 analysis software and the CytoViva 3-D positioning and analysis software for serial section reconstruction. Both the transmission light microscope and EDM were equipped with an Olympus DP73 digital camera with CellSens Dimension camera control and measurement software (Olympus America Inc.; Center Valley, PA). Images for both systems were taken at either high resolution 4800 × 3600 pixels or 2400 × 1800 pixels.

The burden of FSD 8 particles was measured morphometrically in pressure-fixed lungs at 1, 7, 27 and 90 d using enhanced dark-field microscopy of lung tissue sections as described previously (Mercer et al., 1994). Lungs from five animals were measured at each time point. The results were expressed as the volume of particles per unit lung volume.

2.7. FSD 8 particles in the trachea

Experiments were performed to assess whether FSD 8 particles were retained on the tracheal wall following inhalation. In order to preserve the particles in the mucus of the trachea, a sequence of fixatives, which was found previously (Mercer et al., 1991, 1994) to preserve the mucus lining layer in human and rat airways, was applied directly over the trachea. After a 1-day exposure to 30 mg/m^3 FSD 8, rats were euthanized 1, 7 and 27 d post-exposure. A mid-line incision was made in the neck and the trachea was exposed *in situ* by blunt dissection. After creating a compartment to contain the fluid, the trachea was exposed *in situ* to a series of solutions to fix the tissue; these solutions were chosen so as to preserve mucus. The trachea was exposed to 2% glutaraldehyde in 0.84 M sodium cacodylate buffer at pH 7.4 for 30 min; washed with 0.84 M sodium cacodylate with 6% sucrose for 5 min; stained with 2% osmium tetroxide – saline solution adjusted to 350 mosM with sucrose for 15 min; washed for 5 min three times with saline – 6% sucrose to remove unreacted osmium tetroxide; treated with 4% tannic acid – 6% sucrose, pH 7.0 for 15 min; rinsed for 5 min three times with saline – 6% sucrose; stained with 2% uranyl acetate – sucrose solution for 15 min; and stored in sodium cacodylate buffer – 6% sucrose until processed. After fixation, the trachea was removed from the rat and cut into four cylindrical cross sections spanning a region from just below the vocal cords to just above the carina. The four cylindrical cross-sections were then mounted perpendicular to their long axis in a paraffin block and sections were cut at 5 μ thickness. Unstained sections were cover-slipped with Permount. After alignment of the sub-stage oil immersion optics with a 10× objective, sections were examined with 60× air or 100× oil immersion objectives. Enhanced dark-field images were taken with an Olympus DP73 digital camera with CellSens Dimension camera control and measurement software (Olympus America Inc.). Images were taken at 2400 × 1800 pixels.

CellSens Dimension camera software was used to measure the tracheal epithelial thickness of the cylindrical tracheal segments. For each of the four sections of trachea, the thickness of the epithelium from basement membrane to epithelial cell surface was measured at three approximately equal distant points around the circumference of the cylindrical tracheal segment. The mean of the four sections was taken for each animal and results are reported as the mean of the animals for each group.

2.8. In vivo pulmonary mechanics

The purpose of these experiments was to determine whether FSD 8 inhalation affects various parameters of pulmonary function. Pulmonary input impedance of rats was assessed using a flexiVent (SciReq; Montreal, Canada) small animal ventilator system. Animals were anesthetized with ketamine HCl (100 mg/kg; Hospira, Inc.; Lake Forest, IL) and xylazine (10 mg/kg; AnaSed; AKORN Animal Health; Lake Forest, IL) *via* i.p. injection to produce a surgical level of anesthesia. The trachea was exposed through a mid-line incision, and a cannula was advanced a distance equivalent to ~5 cartilage rings and tied in place. Animals were then placed on a ventilator (90 breaths/min; tidal volume, 8 ml/kg; positive end expiratory pressure, 3 cm H_2O). This system interrupts normal ventilation to apply a short, small-amplitude, broad-band volume perturbation at the airway opening. Using the flow and pressure measured at the airway opening, a measurement of pulmonary input impedance was calculated. This measurement was then fit to a model consisting of a Newtonian resistance connected to a constant-phase tissue compartment. Parameters from this model embody energy dissipation in the airways and tissue, and energy storage within the tissue, and can be interpreted in terms of ventilation heterogeneity *vs.* derecruitment and inflammation in the conducting airways *vs.* changes in the lung periphery. The ECG was monitored for changes in heart rate and depth of anesthesia during the period of measurement of respiratory system resistance (R_L and Rrs), elastance (C_{dyn} and Ers), tissue damping

(G), tissue elastance (H), Newtonian resistance (Rn) and hysteresivity (η). Upon completion of the experiment, the rats were euthanized by exsanguination under anesthesia.

2.9. In vivo airway reactivity to MCh

The purpose of these experiments was to determine whether FSD 8 inhalation affects airway reactivity to inhaled MCh (Spectrum Chemical MFG Corp.; New Brunswick, NJ). Rats were anesthetized with ketamine HCl (100 mg/kg) and xylazine (10 mg/kg) given *via* i.p injection. A midline incision was made in the neck, the trachea was exposed, and a cannula was placed into the lumen. Animals received supplemental ketamine HCl (50 mg/kg) by administering the drug topically to the exposed muscle in the neck just before placing the animal into the plethysmograph. Animals were placed on a warming bed in a plethysmograph for the assessment of lung resistance (R_L) and compliance (C_{dyn})[FinePointe RC; Data Sciences International (DSI); St. Paul, MN] and were ventilated using a digital rodent ventilator (Élan Series RC; DSI). Ventilation settings were: maximum mouth pressure, 40 cm H_2O; maximum tidal volume, 3 ml; and respiratory rate, 90 bpm. After recording baseline values of R_L and C_{dyn} and delivery of saline vehicle to obtain baseline values, aerosols of MCh were delivered from 20 μl of solutions of the following concentrations: 0.1, 0.1725, 0.3, 1.0, 1.73, 3.0, 5.75, 10.0 and 17.25 mg/ml. Three, 5-ml (45 cm H_2O mouth pressure) deep inspirations were applied just before each MCh dose was delivered. Maximum R_L (R_{Lmax}) values and minimum C_{dyn} values (C_{dynmin}) were logged at 5-s intervals to quantify R_L and C_{dyn} responses to MCh. Following completion of the experiment, the rats were euthanized by exsanguination under anesthesia.

2.10. In vitro reactivity to MCh: isolated, perfused trachea

The purpose of these experiments was to determine whether airway smooth muscle reactivity to MCh and the modulatory effect of the airway epithelium on reactivity were altered by FSD 8 inhalation. The isolated, perfused trachea preparation has been described in detail (Fedan and Frazer, 1992b; Fedan et al., 2001). After euthanasia, a 25-mm segment of trachea was removed from the rat, cleaned and mounted on a perfusion holder at its *in situ* length. Every effort was made to avoid damage to the epithelium. The holder contained two indwelling, side-hole catheters that were inserted into the lumen and connected to the positive (inlet) and negative (outlet) sides of a differential pressure transducer. The holder, with mounted trachea, was placed into an extraluminal (EL) bath containing modified Krebs-Henseleit solution (MKHS). MKHS contained 113 mM NaCl, 4.8 mM KCL, 2.5 mM $CaCl_2$, 1.2 mM KH_2PO_4, 1.2 mM $MgSO_4$, 25 mM $NaHCO_3$, and 5.7 mM glucose, and was saturated with 95% O_2/5% CO_2, to give pH 7.4 at 37 °C. The trachea was perfused at a constant rate (25 ml/min) with MKHS from a separate bath, the intraluminal (IL) bath, while measuring inlet minus outlet pressure difference (ΔP, cm H_2O) as an index of tracheal diameter. Transmural pressure was set to zero cm H_2O. The MHKS in the IL and EL baths was replaced at 15-min intervals, followed by a 30-min equilibration period during which the MHKS was not changed and the baseline was allowed to become stable. After the equilibration period, MCh was added in stepwise-increasing, cumulative concentrations to the EL bath to induce contractile responses for the generation of concentration-response curves. At the conclusion of the EL concentration-response determination, the EL and IL MKHS was changed at 15-min intervals. Ninety min after the conclusion of the EL concentration-response determination, stepwise-increasing, cumulative concentrations of MCh were added to the IL bath.

The results of these experiments are presented in several ways: 1) the -log[EC50 (M)] values for MCh applied to the EL and IL baths are given along with the maximum contractile responses 2) the EL and IL concentration-response curves are shown with responses normalized in terms of the maximum responses obtained after EL and IL MCh additions, and 3) IL concentration-response curves are presented in a normalized fashion, in which the individual responses evoked in response to the IL additions of MCh are normalized with respect to the maximum response obtained after MCh was added extraluminally. The basis for the latter method of data expression is the fact that the normal relationship between the EL and IL curves is such that the IL curve is normally located on the concentration abscissa to the right of the EL curve over the MCh concentration range, and the IL maximum reponse is smaller than the EL maximum response (Fedan and Frazer, 1992). Treatments that affect epithelial integrity or EpDRF release alter the relationship between the two curves (Fedan et al., 2000), *i.e.*, damage to the epithelium is manifested as a leftward shift of the IL concentration-response curve and an upward shift of the maximum response.

2.11. Electric field stimulation (EFS) of effector nerves

In the rat, airway diameter is under the regulation of intramural cholinergic motor nerves. The purpose of these experiments was to ascertain whether FSD 8 exposure affected effector nerve function by eliciting excitatory neurotransmitter release with EFS and measuring contractile responses of airway smooth muscle (Fedan et al., 2001). After euthanasia, a segment of trachea was removed from the rat, cleaned, and segments, two-cartilage-rings wide, were prepared. Care was taken to avoid damage to the epithelium. The rings were opened by cutting through the cartilage rings opposite the smooth muscle layer to prepare "strips," and suture was tied to each cut end of the cartilage segments. One end of the strip was attached to a holder, and the other end was attached to a force-displacement transducer for the measurement of isometric force. When attached to the holder, the strip was situated between two platinum ring electrodes, one at either end of the strip, for the delivery of EFS. The holder containing the strip was placed in an organ chamber containing MKHS. The strips were placed under 0.6 g basal force. After a 1.5 h-equilibration period, the preparations were stimulated (EFS) with 10-s trains of square-wave pulses of 120 V and 0.5 msec duration and increasing frequency to develop frequency-response curves for the development of contractile responses. There were 5 min between stimulation periods. At the conclusion of the frequency-response determination, the preparations were contracted with 120 mM KCl, and the individual contractions of each tracheal strip were normalized as percentages of the response to KCl, *i.e.*, % KCl. In preliminary experiments, preparations were pre-contracted with 3×10^{-6} M MCh to determine whether relaxation responses could be evoked by stimulation of inhibitory nerves (Fedan et al., 2001); in those experiments relaxation responses were not observed. Thus, only contractile responses were elicited by EFS.

2.12. Epithelial ion transport in isolated tracheal segments

In order to ascertain whether exposure to FSD 8 interfered with epithelial ion transport, following euthanasia tracheal segments were removed from animals, cleaned, and mounted in Ussing chambers in order to measure transepithelial potential difference (V_t), short-circuit current (I_{sc}), and transepithelial resistance (R_t). The apical and basolateral chambers contained MKHS solution. The epithelium was allowed to reach a stable V_t under open-circuit conditions before applying a 0 mV-voltage-clamp across Ag/AgCl electrodes (4% agar in MKHS) in order to record I_{sc} (μA/cm^2), an index of active ion transport, using an EVC 4000 automatic voltage/current amplifier (World Precision Instruments; Sarasota, FL). Square-wave voltage pulses (1 mV, 5 s duration) were delivered every 55 s to yield a voltage response for calculation of R_t, an index of paracellular permeability, from Ohm's law.

To investigate the possible involvement of FSD 8-induced changes in epithelial Na^+ and Cl^- channels and the Na^+,K^+-pump, the effects of the following inhibitors were evaluated: apical amiloride (3×10^{-5} M) to block apical membrane Na^+ channels, apical 5-nitro-2-(3-phenylpropylamino) benzoic acid (NPPB; 10^{-4} M) to block apical membrane Cl^-

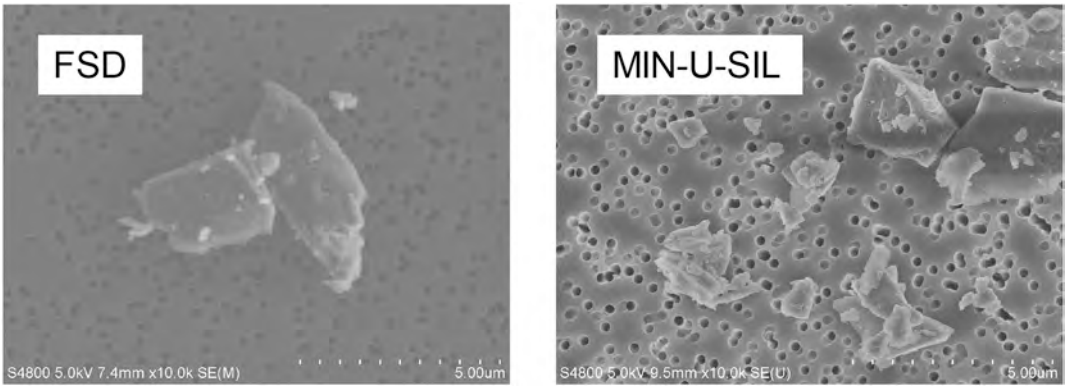

Fig. 3. Representative FSD 8 and MIN-U-SIL particles showing small particles adherent to larger particles on comparably sized particles.

channels, and ouabain (10^{-4} M) to block the basolateral membrane Na^+, K^+-pump. Amiloride was dissolved in saline; NPPB and ouabain were dissolved in dimethyl sulfoxide (DMSO); all inhibitors were from Sigma-Aldrich (St. Louis, MO). The effects of these agents were characterized with regard to I_{sc} responses they initiated and their effects on R_t.

2.13. Normal human bronchial epithelial cells (NHBEs): Ion transport, lactate dehydrogenase (LDH) release and cytokine release

NHBEs were cultured in air liquid interface to ascertain whether incubation with FSD 8 affected ion transport or caused cell damage. NHBEs (CC-2540S; Lonza, Inc.; Walkersville, MD) were grown using a Clonetics B-ALI™ BulletKit (00193514, Lonza). Cells were expanded into a T-75 flask containing Clonetics B-ALI™ growth medium. Medium was changed after 24 h and every 48 h thereafter. Cells were harvested on day 4 or after they had become >80% confluent. Cells were detached with 0.025% Trypsin-EDTA (Stemcell Technologies; Vancouver, BC) and seeded into collagen coated 24-well transwell plates (Corning 3470) at >75,000 cells/well using B-ALI™ growth medium. On day 3, air-interface culture began with removal of the growth media from the upper and lower chamber and addition of B-ALI™ differentiation medium in the lower chamber only. Medium was replaced every 48 h in the lower (basolateral) chamber while maintaining air exposure in the upper (apical) chamber. On day 20, the presence of mucus was confirmed by Alcian blue (Sigma-Aldrich) staining. The presence of cilia was confirmed with anti-β-tubulin antibody (ab6046; ABCAM, Cambridge, MA) and fluorescence microscopy. On day 24, epithelial integrity was confirmed from transepithelial resistance (TEER) measurement of >1000 Ω using an Endohm (World Precision Instruments; Sarasota, FL); the TEER values ranged from 1200 to 2800 Ω.

After reaching >1000 Ω, 50 μl of FSD 8 particles suspended in B-ALI™ differentiation medium (Lonza) were applied in varying concentrations (0.0001–1 mg/well) to the apical surface of the NHBEs. Control cells received 50 μl of B-ALI™ medium. Eighteen h later, the cells were mounted in Ussing chambers for the measurement of V_t, R_t and I_{sc} and bioelectric responses to amiloride, NPPB and ouabain.

For measurement of LDH and cytokine release from NHBEs, the apical chamber was washed with 100 μl B-ALI™ differentiation medium and all media (~150 μl, apical; 500 μl, basolateral) were recovered and samples were kept on ice. LDH activity was assayed in the apical and basolateral media using a Cobas MIRA analyzer (Roche Diagnostics USA; Indianapolis, IN). LDH activity was quantified by detection of the oxidation of lactate coupled to the reduction of NAD^+ at 340 nm. Results in LDH units per ml were converted to LDH activity/insert. Assay of released cytokines utilized the Human Cytokine Array/Chemokine Array 65-Plex Panel (HD65) and was performed by Eve Technologies (Calgary, AB).

2.14. Measurement of vascular permeability using Evans blue dye

The purpose of these experiments was to investigate the effects of FSD 8 exposure on vascular permeability of airway blood vessels using capsaicin-induced Evans blue dye extravasation. Evans blue dye binds tightly to albumin after i.v. injection and appears in extravascular tissues if vascular permeability is increased; otherwise, Evans blue normally remains in the vascular compartment.

Following an i.p. injection of ketamine HCl (100 mg/kg) plus xylazine (10 mg/ml), a ventral, left of mid-line neck incision was used to isolate and cannulate the jugular vein. An i.v. injection of 30 mg/kg Evans blue dye was infused followed 5 min later by an i.v. injection of capsaicin (75 μg/kg; Sigma-Aldrich). Control animals (air- or FSD 8-exposed) did not receive capsaicin. Five min after capsaicin was given, the abdomen was opened, the rat was exsanguinated, and the thoracic aorta was catheterized retrogradely. The inferior vena cava was tied off to limit perfusion to the upper body and a small hole was cut in the left atrium. The animal was perfused with 0.25 ml/g saline over 2 min to flush excess dye from the bronchial and pulmonary vasculature. The trachea, intrapulmonary airways and lung were removed, and Evans blue was extracted in formamide. Evans blue concentration was measured in a photometer at 620 nm, calibrated to a standard curve, and recorded as mg Evans blue/mg wet tissue.

2.15. Statistical analysis

The results are expressed as mean ± standard error. For pulmonary mechanics and airway reactivity to MCh *in vivo* experiments, and isolated, perfused trachea, EFS, and Ussing chamber experiments, *n* values are given in the figure legends or in the tables. The data were analyzed for differences using SAS version 9.4 for Windows (SAS Institute, Cary NC). Data were modeled with Proc Mixed using a two-way mixed-model factorial (FSD 8 exposure by MCh or KCl stimulation depending on the experiment) analysis of variance with repeated measures on the MCh/KCl stimulation. Treatment comparisons at each MCh concentration were generated using the "slice" and "pdiff" options in Proc Mixed. Effective MCh concentrations giving 50% of the maximum response (EC50; −log M) in isolated, perfused trachea experiments were calculated using a 4-parameter logit curve fit of logarithmically-transformed values, which are normally distributed. The results were analyzed for differences using analysis of variance (ANOVA). For all analyses $P < 0.05$ was regarded as significant.

The Eve Technologies Cytokine Array/Chemokine Array 65-Plex Panel was analyzed using SAS v9.4 (SAS Institute) for Windows. Data were log transformed prior to analysis. Data were analyzed using the dose as a continuous variable to evaluate the slope of the dose-response curve, and as a categorical variable to compare individual groups with the control using Dunnett's test for *post hoc* comparisons. Analyses were

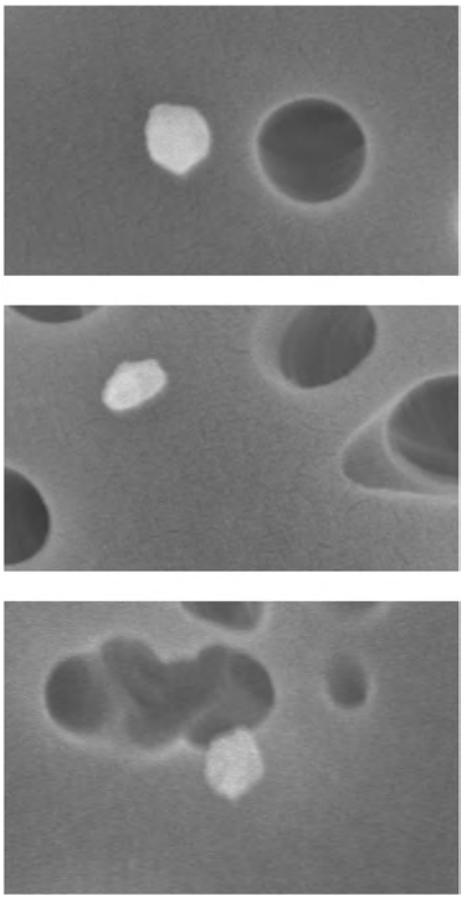

Fig. 4. Representative FSD 8 particles of approximately 100 nm diameter.

performed using Proc Mixed in both cases. All slopes were considered significantly different from 0, and comparisons to controls were considered significant at $P < 0.05$.

All other analyses were performed using ANOVA or Student's *t*-tests, as appropriate.

3. Results

3.1. Animal well-being and body weights

Animals experienced no discomfort during and after the FSD 8 inhalation exposures. Inhalation of FSD 8 had no effect on weight gain during the 90-d period following exposure to 10 or 30 mg/m^3 of the dust (Fig. S1).

3.2. FSD 8 inhalation exposure system

The inhalation exposure system was computer-controlled and reliably generated aerosols of FSD 8 at constant concentrations of 10 and 30 mg/m^3 for at least 6 h (Fig. 2). The system utilized a two-stage generation method to aerosolize and disperse the FSD 8. The first stage consisted of an acoustical aerosol generator which fed FSD to the second stage, a venturi disperser that increased the dispersion of aggregated particles before the aerosol entered the animal exposure chamber. The desired FSD 8 aerosol levels were reached within ~20 min following placement of the animals into the exposure chamber and remained constant thereafter during the 6-h exposure period. Particle concentrations inside the exposure chamber were verified daily by gravimetric analysis. The average of all the 4 d exposures to 10 mg/m^3 FSD was 9.99 ± 0.27 mg/m^3; the average of all the 4 d exposures to 30 mg/m^3 FSD was 29.71 ± 0.76 mg/m^3 (means±standard deviations).

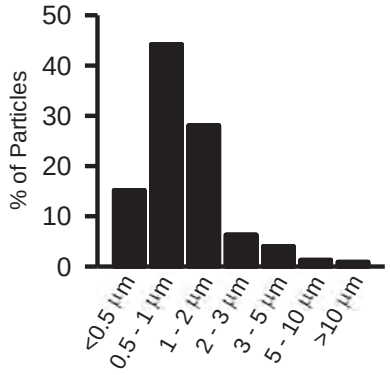

Fig. 5. Size distribution of FSD 8 particles measured optically. The sizes indicated are those of the particles' major axis.

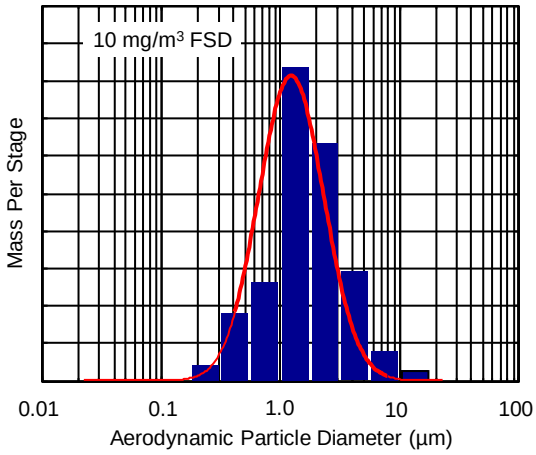

Fig. 6. Aerodynamic mass size distribution of FSD 8 determined with MOUDI. The mass geometric mean ± standard error was 1.75 ± 2.4 µm.

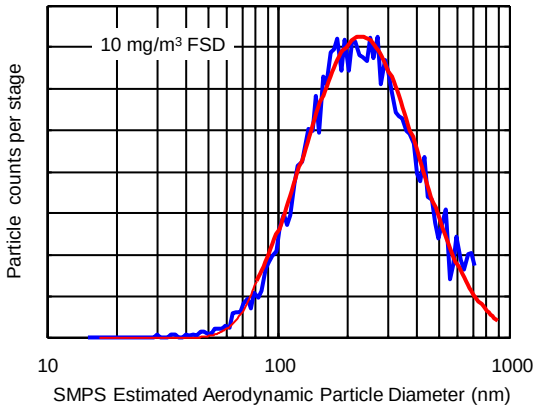

Fig. 7. SMPS estimated aerodynamic FSD 8 particle diameter count size distribution. The count geometric mean ± standard error was 227 ± 1.7 nm.

3.3. Particle size of neat FSD 8 vs. MIN-U-SIL

SEM images of neat FSD 8 particles in comparison to MIN-U-SIL particles were obtained and reported in Fedan et al. (2020). MIN-U-SIL has been used widely in investigations into quartz dust toxicity.

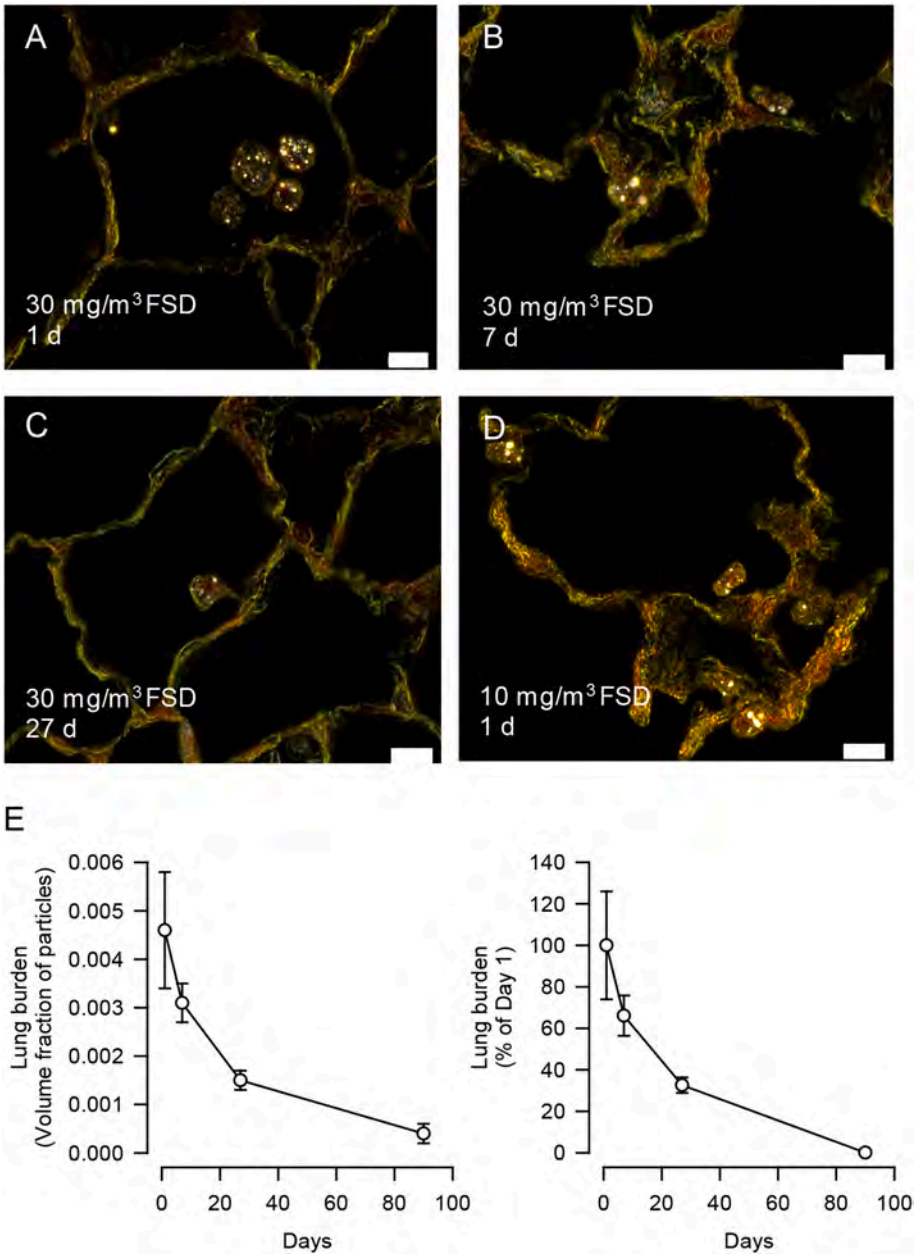

Fig. 8. FSD 8 clearance rates from the lung. A, Enhanced dark-field image of the alveolar region at 1 d post-exposure after 30 mg/m^3 FSD 8 exposure. B, Enhanced dark-field image of the alveolar region at 7 d post-exposure after 30 mg/m^3 FSD 8 exposure. C, Enhanced dark-field image of the alveolar region at 27 d post-exposure after 30 mg/m^3 FSD 8 exposure. D, Enhanced dark-field image of the alveolar region at 1 d post-exposure after 10 mg/m^3 FSD 8 exposure. E, Lung burden of FSD 8 based on the 30 mg/m^3 FSD 8 exposure in terms of volume fraction of particles and percentage measured on day 1.

The neat FSD 8 sample contained a wide range of particle sizes, whereas the MIN-U-SIL 5 particles were of more uniform size because they had been selected *a priori* to be ≤5 μm. For particles of ≤5 μm size there were no obvious differences evident in the shapes of the particles. Fig. 3 illustrates that for both FSD and MIN-U-SIL small, individual particles of many sizes were present; in addition, small particles were adherent to large particles in both cases. Individual nanoparticles (~100 nm) also were observed (Fig. 4).

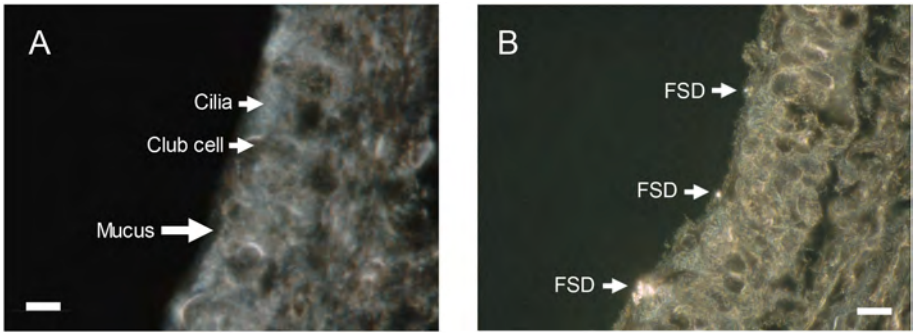

Fig. 9. A, Enhanced dark-field image of unstained tracheal wall from filtered air-exposed rats showing the epithelium and mucus layer. A layer of preserved mucus (large arrow) can be seen above the epithelial cells. In different regions, the mucus is intermixed with cilia (small arrow) and the domes of club cells. Bar = 5 μ. B, Enhanced dark-field image of unstained tracheal wall showing FSD 8 particles in mucus at 1 d following exposure to 30 mg/m^3 FSD 8. The image demonstrates one large cluster of FSD 8 particles and two smaller FSD 8 particles above the epithelium of the trachea (white arrows). No significant particles were associated with the epithelium at post-exposure days 7 or 27. Bar = 10 μm.

Table 1
Tracheal epithelium thickness following inhalation of filtered air or 30 mg/m^3 FSD 8.

Treatment	Days post-exposure	Thickness (μ)
Filtered air	1	8.98 ± 0.38
	7	9.40 ± 0.88
	28	10.07 ± 0.70
FSD 8-exposed	1	9.32 ± 0.54
	7	8.87 ± 0.56
	28	10.08 ± 0.77

Optical measurements of FSD 8 particles in SEM fields provided information about the FSD particles' actual sizes. The results are shown in Fig. 5, in which it may be seen that particles ranged in physical size from <0.5 μm to >10 μm. Particles 0.5–1 μm were the most prevalent.

MOUDI analysis of aerodynamic particle diameter in aerosols generated from 10 mg/m^3 FSD 8 indicated that the mass median aerodynamic particle diameter (MMAD) was 1.75 ± 2.4 μm (geometric mean ± standard deviation; Fig. 6). SMPS analysis revealed an estimated count median aerodynamic particle diameter (CMAD) of 227.0 ± 1.7 nm (mean ± standard deviation; Fig. 7). The findings indicate that a bulk of FSD 8 particles in the aerosol generation system fell in the respirable range.

3.4. Lung weights

Fig. S2 illustrates that inhalation of 10 or 30 mg/m^3 FSD 8 had no effects on lung wet weights, dry weights, or the dry weight/wet weight ratios, at 1, 7 and 27 d post-exposure.

3.5. FSD 8 lung clearance analysis: enhanced dark-field microscopy

Enhanced dark-field microscopic imaging of sections taken from pressure-fixed lung tissue from 1, 7, 27, and 90 d post-exposure to 30 mg/m^3 FSD 8 was used to calculate the half-life of the FSD 8 particles in the lungs over the course of the post-exposure time-period, in addition to providing images of the particles in the lungs (Fig. 8). FSD 8 was observed in the lungs at 1 d post-exposure. At later time points, FSD 8 was found within alveolar macrophages. No cell-free particles were observed in lungs from 10- or 30 mg/m^3-exposed groups. FSD 8 clearance from the lungs was rapid and efficient, as evidenced by a calculated clearance half-life of 11.3 d. No significant difference in half lives, other than the difference in initial lung burden assessed microscopically, occurred in the lungs from animals exposed to either dose of FSD 8 (data not shown).

3.6. FSD 8 particles in the trachea

An enhanced dark-field microscope image of an unstained tracheal epithelium from a filtered air-exposed rat is shown in Fig. 9A. The immersion fixation of the trachea *in situ* was found to preserve the mucus layer of the trachea except in those areas where there was obvious mechanical disruption due to excision of the trachea from the animal after fixation. The different regions of the mucous lining layer can be seen intermixed with cilia and the domes of Club cells.

Fig. 9B is a representative image of the observations of FSD 8

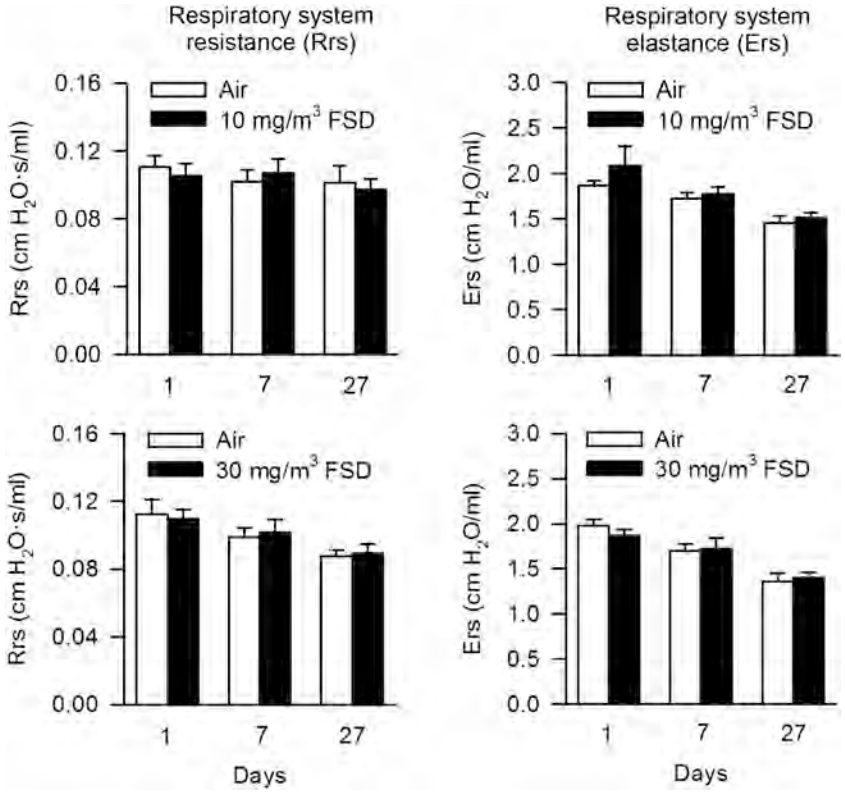

Fig. 10. Effect of inhalation of 10 mg/m^3 and 30 mg/m^3 FSD 8 on respiratory system resistance (left panel) and respiratory system elastance (right panel) 1, 7 and 27 d post-exposure. $n = 8$ animals per group per time point. FSD 8 had no effect on these parameters. Additional parameters (Newtonian resistance, hysteresivity, tissue damping, and tissue elastance) are presented in Figs. S3 and S4.

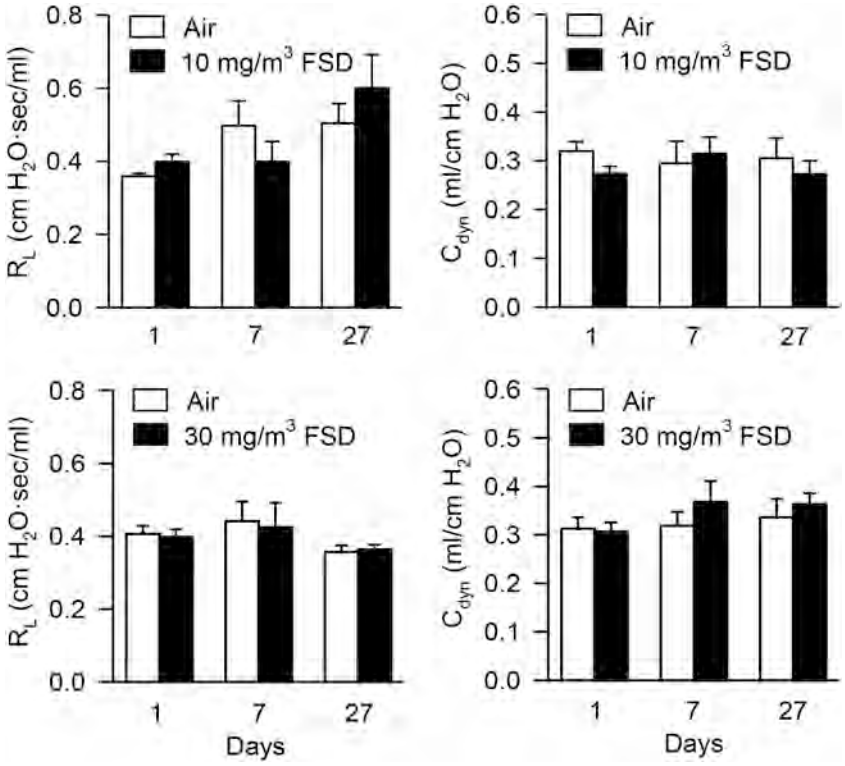

Fig. 11. Effect of inhalation of 10 and 30 mg/m^3 FSD 8 on basal R_L and C_{dyn} 1, 7 and 27 d post-exposure. *n* values were as follows: for 10 mg/m^3, contol, $n = 7$, 6 and 8, and FSD 8, $n = 6$, 7, and 8, respectively, for 1, 7 and 27 d post-exposure periods; for 30 mg/m^3, control, $n = 12$, 8 and 5, and FSD 8, $n = 8$, 8, and 7, respectively, for 1, 7 and 27 d post-exposure periods. FSD 8 had no effect on these parameters.

particles in the tracheal mucus 1 d after exposure to 30 mg/m^3 FSD 8. FSD 8 particles were present in larger concentrated clusters of 5–10 particles or as isolated particles. In general, FSD 8 particles were relatively few, with only one or two such cases for each cylindrical tracheal profile at 1 d post-exposure. FSD 8 particles were rarely observed at 7 and 27 d.

Results from measurement of the tracheal epithelial thickness are given in Table 1. On average, the epithelial thickness of the trachea varied from 9 to 10 μm in the filtered air-exposed control animals and was not altered significantly by exposure to FSD 8 particles at 1, 7 or 27 d post-exposure.

3.7. Effect of FSD 8 inhalation on in vivo pulmonary mechanics and regulation of breathing

Fig. 10 depicts the effects of FSD 8 inhalation on respiratory system resistance (Rrs) and respiratory system elastance (Ers). The effects of FSD 8 tissue damping (G), tissue elastance (H), Newtonian resistance (Rn) and hysteresivity (η) are shown in Figs. S3 and S4. Compared to air-breathing controls, inhalation of 10 mg/m^3 FSD 8 had no effect on Rrs, Ers, G, H, Rn or η, 1, 7 or 27 d after inhalation (Figs. 10 and S3). Likewise, inhalation of 30 mg/m^3 FSD 8 was without effect (Figs. 10 and S4). These results indicated that FSD 8 inhalation had no effect on pulmonary mechanics.

3.8. Effect of FSD 8 inhalation on in vivo airway reactivity to MCh

Fig. 11 illustrates that exposure to 10 or 30 mg/m^3 FSD 8 had no effect on basal R_L or C_{dyn} at 1, 7 and 27 d post-exposure, in agreement with the findings in Section 3.6.

To investigate whether inhalation of FSD 8 affected airway reactivity to MCh, following recording of basal R_L and C_{dyn}, the animals were challenged *via* inhalation with increasing doses of MCh and changes in R_L and C_{dyn} compared to basal values were recorded. The results are expressed as percent change from basal values (%ΔR_L and %ΔC_{dyn}) in Figs. 12 and 13. Reactivity to MCh (R_L) was unaffected at 10 mg/m^3 FSD 8, but was increased significantly at lower MCh doses following inhalation of 30 mg/m^3 FSD 8; the increases in responses were small but the MCh dose-response curve was shifted to the left after 7 d post-exposure. At 27 d post-exposure, reactivity to MCh was increased significantly at the highest MCh dose (R_L). Seven d after inhalation of 10 mg/m^3, but not 30 mg/m^3 FSD 8, C_{dyn} responses to MCh were blunted significantly compared to the air-breathing controls, and the dose-response curve was shifted to the left, indicative of airway hyperreactivity. The raw data from which the normalized values of R_L and C_{dyn} were derived are found in Figs. S5 and S6.

3.9. Effect of FSD 8 inhalation on in vitro reactivity to MCh: isolated, perfused trachea

The isolated, perfused trachea preparation was utilized to determine whether FSD 8 inhalation affected reactivity of the airway smooth muscle or the diffusion barrier function/modulatory role of the epithelium on reactivity. In the first case, reactivity of the airway smooth muscle was assessed by administering MCh to the extraluminal (EL) bath, where the drug has immediate access to the smooth muscle on the exterior surface of the airway. In the second case, the diffusion of MCh across the airway wall to reach the muscle after the agonist has been applied to the intraluminal (IL) bath is hindered by the epithelial barrier, and contractile responses are modulated by epithelium-derived relaxing factor (EpDRF); an effect on the diffusion barrier or modulatory effect of EpDRF are manifested as a change in the position of the IL MCh concentration-response curve.

Inhalation of 10 mg/m^3 FSD 8 reduced reactivity to EL MCh

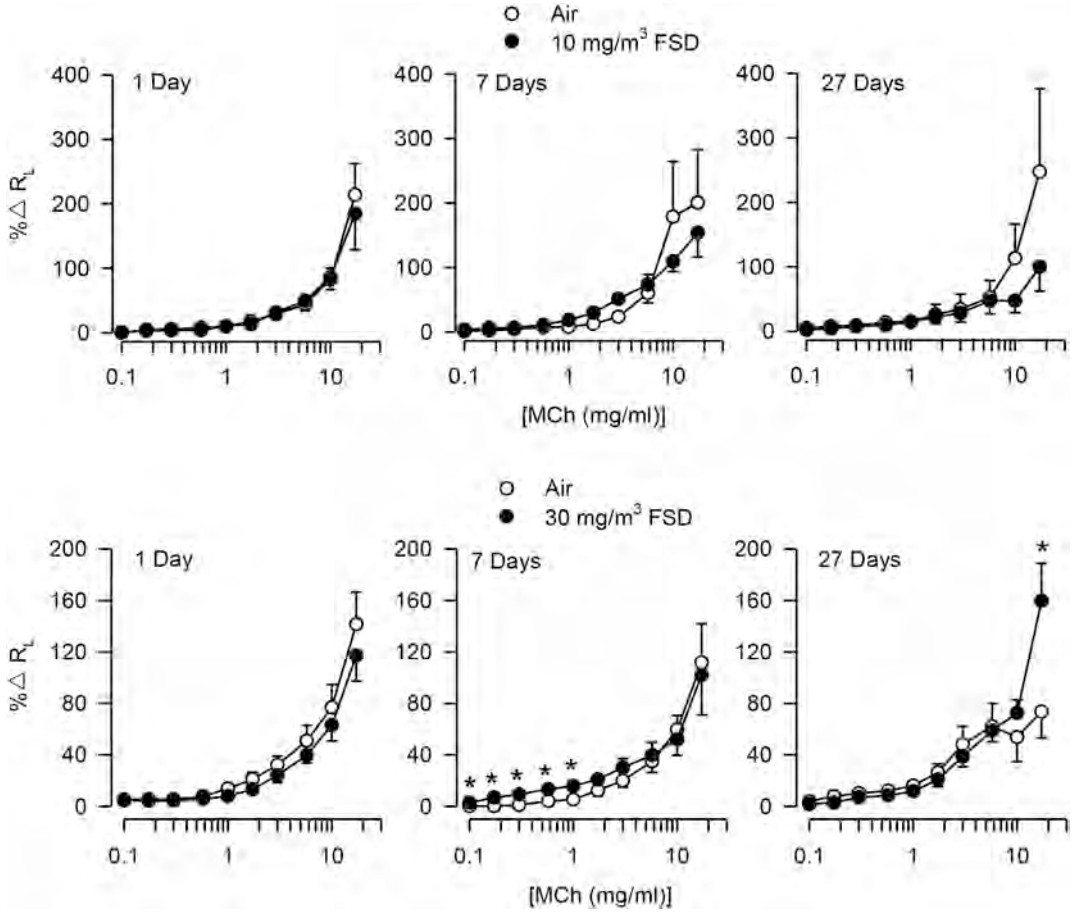

Fig. 12. Effect of inhalation of 10 and 30 mg/m^3 FSD 8 on R_L responses to inhaled MCh aerosol 1, 7 and 27 d post-exposure. *n* values were as follows: for 10 mg/m^3, contol, $n = 7$, 6 and 8, and FSD 8, $n = 6$, 7, and 8, respectively, for 1, 7 and 27 d post-exposure periods; for 30 mg/m^3, control, $n = 12$, 8 and 5, and FSD 8, $n = 8$, 8, and 7, respectively, for 1, 7 and 27 d post-exposure periods. These results depict changes in R_L from basal values in response to MCh (Fig. 12). $^*P < 0.05$, air-breathing controls *vs.* FSD 8-exposed. The raw data from which these results were normalized is presented in Fig. S5.

appreciably 7 d following exposure (Fig. 14; Table 2). Reactivity to IL MCh was increased at 7 d following exposure (Table 2). The 30 mg/m^3 dose had no effect on reactivity to EL MCh. However, there was a slight effect on responses to IL MCh at 7 d following exposure that is likely biologically meaningless (Fig. 14; Table 2).

In the isolated, perfused trachea preparation, ΔP varies with the 5th power of the radius. The initial diameter of the trachea while in the apparatus, under a standard, fixed rate of perfusion with MKHS through the lumen, sets the basal value of ΔP, which is then beyond the control of the investigator. Responses to a given contractile agonist are enlarged in preparations with a high basal Δ*P* value compared to those with low Δ*P* values. To evaluate further whether exposure to FSD 8 altered the relationship between EL and IL MCh concentration-response curves [see Fedan and Frazer (1992)], the results were expressed in terms of the IL responses to MCh normalized in terms of the EL maximum response, *i.e.*, %EL maximum response. Fig. 15 illustrates that, 7 d after inhalation of 10 mg/m^3 FSD 8, the relationship between the EL and IL MCh concentration-response curves was altered, *i.e.*, the maximum response to IL MCh as a percentage of the EL maximum response, normally 60–80%, was potentiated significantly. Subsequently, this effect waned in time. This finding suggested that the epithelial barrier function and/or modulation of responsiveness by EpDRF were lessened after FSD 8 inhalation at this dose and post-exposure period. Exposure to 30 mg/m^3 FSD 8 led to a reduction in IL maximum response relative to the EL maximum response at one d post-exposure (Fig. 15); this effect did not occur at the later time points. Thus, whereas significant effects of FSD 8 were observed, the changes did not occur along a continuum, but depended upon the FSD 8 inhalation dose and the post-exposure period.

3.10. Effect of FSD 8 inhalation on neurogenic contractile responses elicited with EFS

Contractions of tracheal strips were evoked with EFS to stimulate neurotransmitter-induced contractile responses. Following exposure to 10 mg/m^3 FSD 8, neurogenic responses of the preparations were unaffected by the exposures. However, at 30 mg/m^3 FSD 8, there was a small but significant, perhaps biologically insignificant, increase at 30 Hz 7 d following exposure (Fig. 16). This finding suggests that the release of acetylcholine from parasympathetic, postganglionic neurons and/or postjunctional muscarinic receptors may have been affected slightly by 30 mg/m^3 FSD 8 exposure which waned by 27 d following exposure.

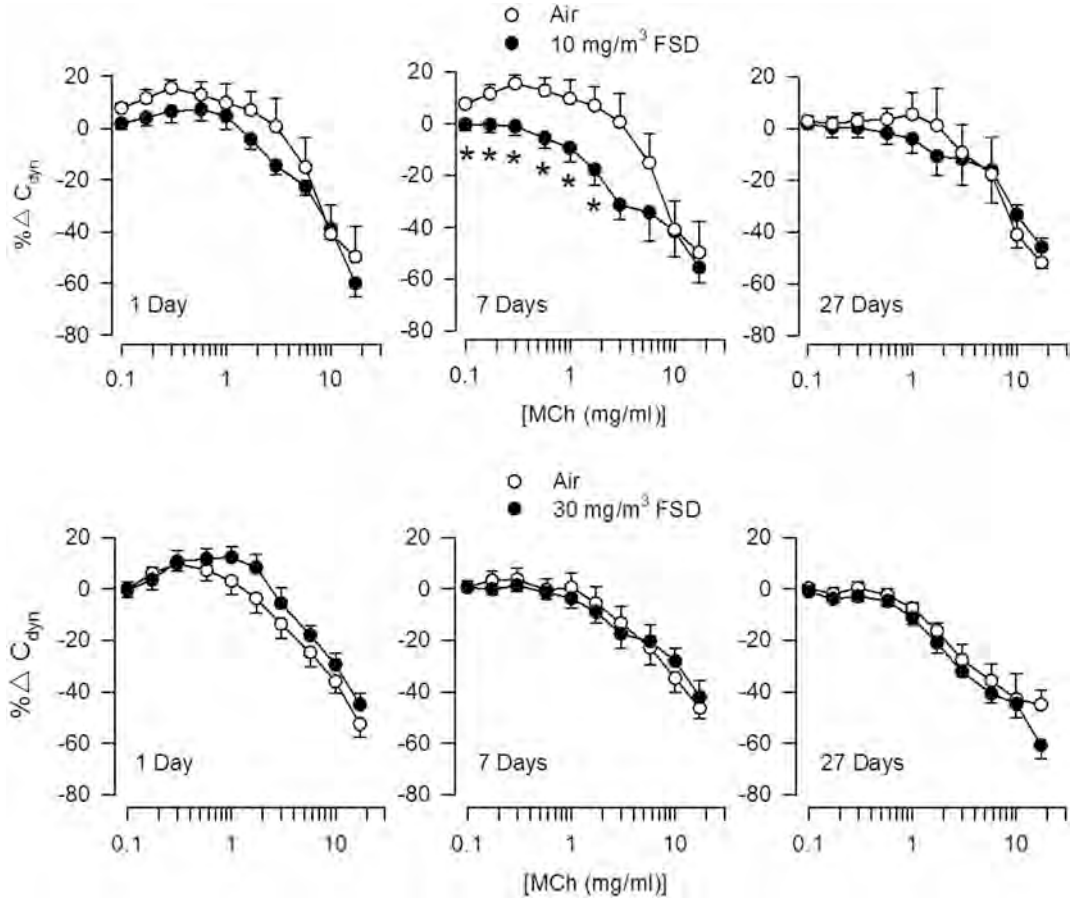

Fig. 13. Effect of inhalation of 10 and 30 mg/m^3 FSD 8 on C_{dyn} responses to inhaled MCh aerosol 1, 7 and 27 d post-exposure. *n* values were as follows: for 10 mg/m^3, contol, $n = 7$, 6 and 8, and FSD 8, $n = 6$, 7, and 8, respectively, for 1, 7 and 27 d post-exposure periods; for 30 mg/m^3, control, $n = 12$, 8 and 5, and FSD 8, $n = 8$, 8, and 7, respectively, for 1, 7 and 27 d post-exposure periods. *$P < 0.05$, air-breathing controls *vs.* FSD 8-exposed. These results depict changes in C_{dyn} from basal values in response to MCh (Fig. 12). The raw data from which these results were normalized is presented in Fig. S6.

3.11. Effect of FSD 8 on vascular permeability in the lung

Whether an increase in vascular permeability mediated by neurogenic inflammation occurred in the lung following exposure to FSD 8 was examined using the Evans blue dye extravasation method. If vascular permeability has been increased, the appearance of the dye in the extravascular compartment in response to capsaicin is enhanced compared to control, owing to the greater release of neuropeptides that increase vascular permeability. Fig. 17 illustrates that the dye appeared in the extravascular compartment of tracheas, bronchi and lungs of air-breathing control animals. There were no differences in the levels of extravasated Evans blue dye in the controls. Following administration of capsaicin in both the air-breathing and 30 mg/m^3 FSD 8-exposed animals (the 10 mg/m^3 FSD 8 dose was not tested in this series of experiments), additional dye entered the vasculature. However, the responses to capsaicin were not affected by FSD 8 inhalation at 1, 7 and 27 d post-exposure compared to air-breathing controls, signifying that the dust had not caused an increase in vascular permeability in the trachea, bronchi or lungs.

3.12. Effect of FSD 8 inhalation on epithelial ion transport

Inhalation of 10 or 30 mg/m^3 FSD 8 had no effect on basal V_t, I_{sc} or R_t at 1, 7 and 27 d post-exposure (Fig. 18). The effects of FSD 8 treatment on epithelial Na^+ and Cl^- channels were assessed by examining the inhibitory effects of amiloride (apical Na^+ channel blocker), NPPB (apical Cl^- channel blocker), and ouabain (Na^+,K^+-pump inhibitor) on I_{sc} and R_t of tracheal segments *in vitro*. The results of these experiments are presented both in normalized terms (% change in R_t and I_{sc} from basal values) as well as the raw data from which the % change data were normalized. As shown in Fig. S7 (normalized results) and Fig. S8 (raw data), 10 mg/m^3 FSD 8 exposure had no effect on I_{sc} or R_t responses to amiloride, NPPB or ouabain at 1, 7 and 27 d post-exposure. In contrast, following inhalation of 30 mg/m^3, the inhibitory effect of amiloride on I_{sc} was attenuated significantly at 1, 7 and 27 d post-exposure (Fig. 19, normalized data; Fig. S9 raw data). In the absence of an effect of amiloride on R_t (Figs. 19), these findings indicate that FSD 8 exposure resulted in an attenuated inhibitory effect of amiloride on Na^+ channels in trachea preparations. In contrast, responses to NPPB were unaffected by FSD 8 inhalation. At 7 d post-exposure, the inhibitory effect of ouabain on I_{sc} was reduced significantly.

3.13. Effects of FSD 8 on NHBEs

3.13.1. Ion transport

In order to determine whether epithelial ion transport *in vitro* also was altered after exposure to FSD 8, primary NHBE cells were exposed to increasing doses of FSD 8 (0.0001–1 mg/well) and responses to ion

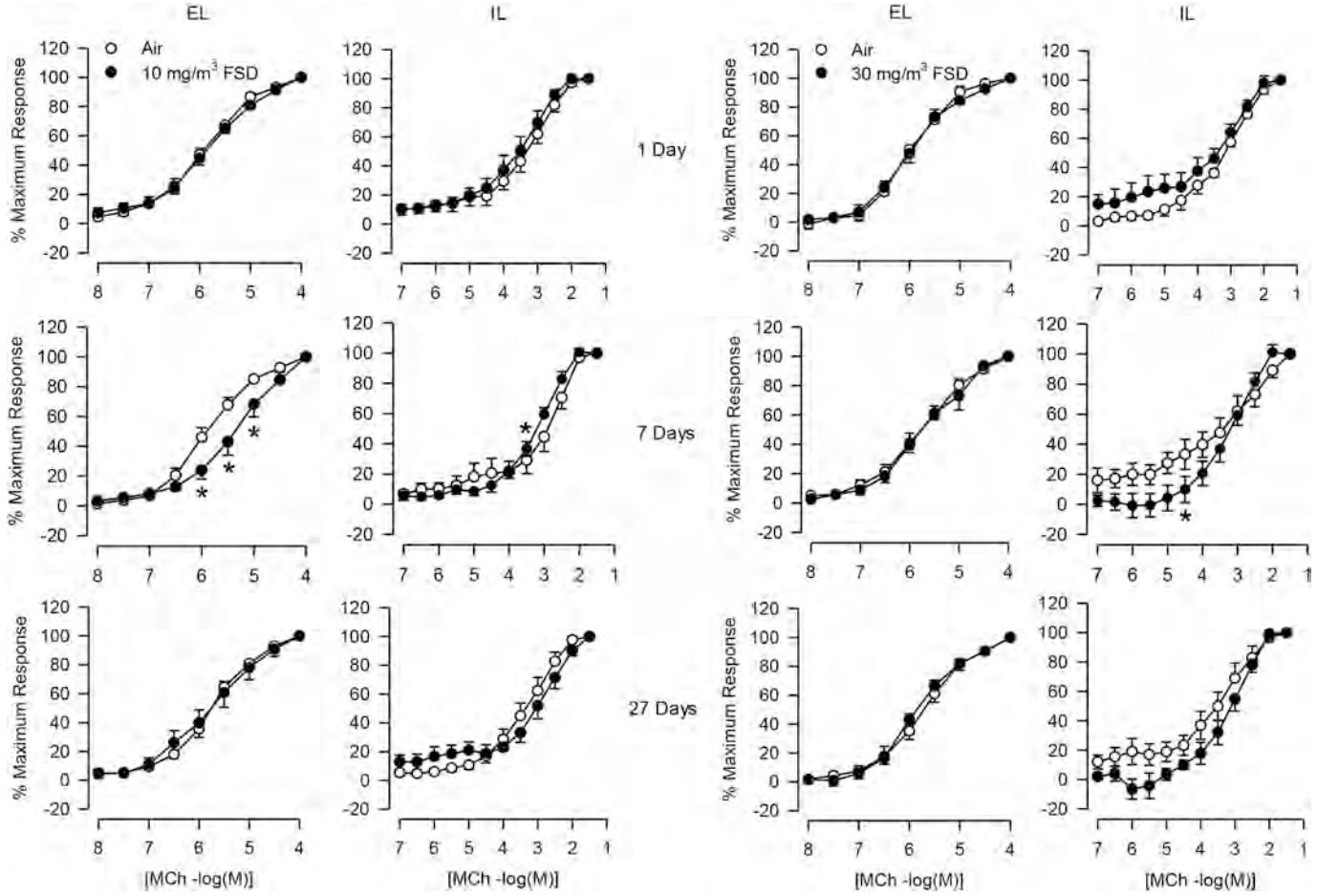

Fig. 14. Reactivity of the isolated, perfused trachea preparation to MCh applied to the EL and IL baths, 1, 7 and 27 d following exposure to 10 (left six panels) and 30 mg/m^3 (right six panels) FSD 8. In this figure, the responses to MCh are plotted in terms of the maximum contractile response for the EL curve and the IL curve. In each cluster, the panels in the left column depict concentration-response curves obtained following the cumulative additions of MCh to the EL bath; the panels in the right column depict concentration-response curves obtained following the cumulative additions of MCh to the IL bath. For each FSD 8 dose and post-exposure time point the EL and IL curves were both obtained from each trachea. *n* values were as follows: for 10 mg/m^3, EL curves, $n = 8$, 4 and 6, and IL curves, $n = 5$, 5, and 5, respectively, for 1, 7 and 27 d post-exposure periods; for 30 mg/m^3, EL curves, $n = 5$, 6 and 5, and IL curves, $n = 5$, 6, and 5, respectively, for 1, 7 and 27 d post-exposure periods. *$P < 0.05$, air-breathing controls *vs.* FSD 8-exposed.

Table 2
Reactivity of isolated, perfused trachea to MCh added to the extraluminal or intraluminal bath following inhalation of filtered air or 10 or 30 mg/m^3 FSD 8.

Treatment	Days post-exposure	-log[EC50 (M)]	
		Extraluminal	Intraluminal
10 mg/m^3 FSD 8			
Filtered air	1	5.77 ± 0.14	3.59 ± 0.37
FSD 8-exposed	1	5.92 ± 0.12	3.59 ± 0.26
Filtered air	7	5.92 ± 0.14	2.65 ± 0.16
FSD 8-exposed	7	5.33 ± 0.19*	3.16 ± 0.08*
Filtered air	27	5.71 ± 0.08	3.31 ± 0.20
FSD 8-exposed	27	5.73 ± 0.33	3.06 ± 0.17
30 mg/m^3 FSD 8			
Filtered air	1	5.98 ± 0.07	3.09 ± 0.05
FSD 8-exposed	1	5.89 ± 0.11	3.13 ± 0.10
Filtered air	7	5.79 ± 0.18	3.14 ± 0.46
FSD 8-exposed	7	5.73 ± 0.12	3.55 ± 0.17
Filtered air	27	5.96 ± 0.34	3.20 ± 0.20
FSD 8-exposed	27	5.87 ± 0.09	3.14 ± 0.17

Filtered air *vs.* FSD 8-exposed, *$P < 0.05$.

transport inhibitors were assessed in Ussing chambers. The NHBEs exhibited increases in both V_t and R_t in response to incubation with FSD 8 (Fig. 20). The increases in R_t suggest that decreases in ion transport through the tight junctions were produced by treatment with FSD 8. There were no significant changes in apical Na^+, or Cl^- transport, or Na^+,K^+-pump activity, at either dose of FSD 8 (Fig. S10), as judged from the lack of effects of FSD 8 on responses to amiloride, NPPB and ouabain. Other pathways are, apparently, contributing to the increases in V_t and R_t, and further work is needed to identify them.

3.13.2. LDH release and cytokine release

Experiments were conducted to determine whether FSD 8 caused cytotoxic or pro-inflammatory effects in NHBEs. Cytotoxicity was assessed by measuring LDH levels in apical and basolateral media. No LDH was released into the basolateral medium; that is, the level of the enzyme was below the limit of detection. LDH was released into the apical medium, however, and its level was unaffected by incubation with FSD 8 (Fig. 21), suggesting that cytotoxicity had not been evoked by the dust.

3.13.3. Cytokine release

The release of cytokines into apical and basolateral media in response to incubation with FSD 8 was assessed using a 65-cytokine

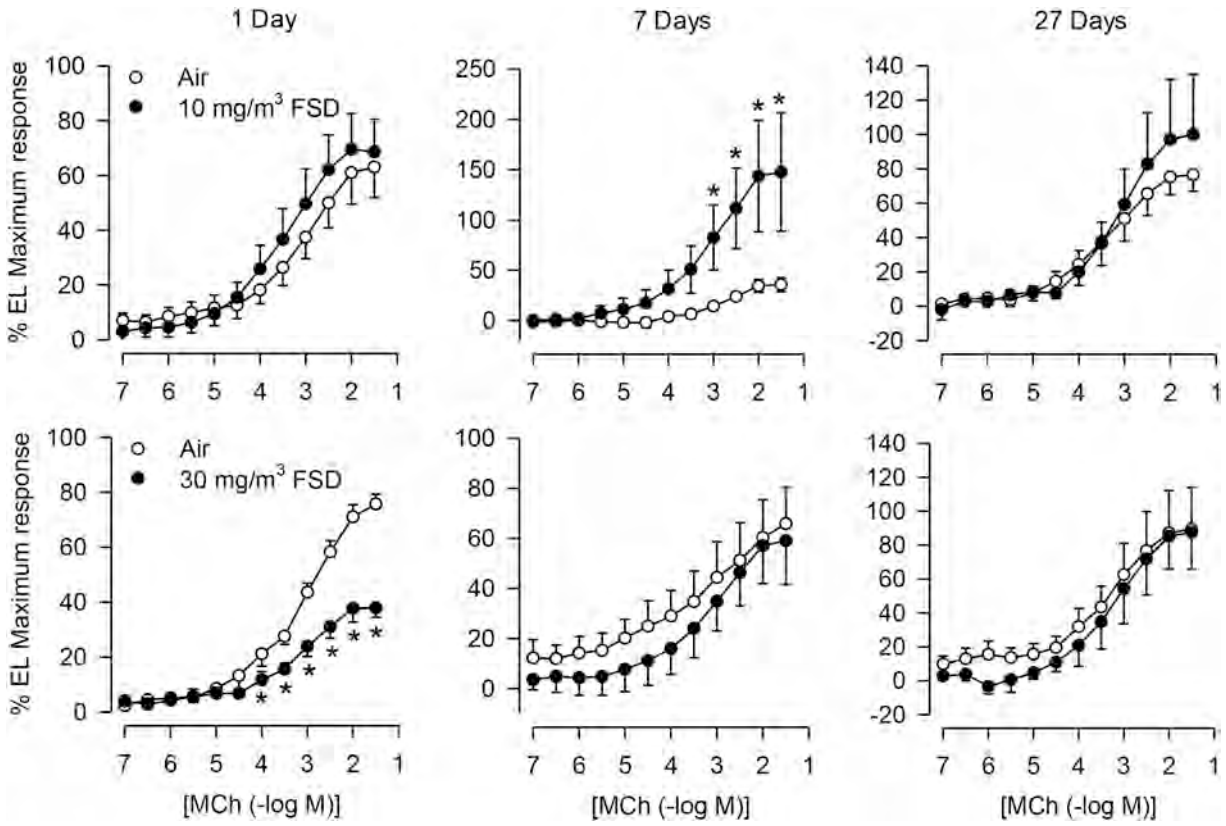

Fig. 15. Reactivity of the isolated, perfused trachea preparation to MCh applied to the IL bath, 1, 7 and 27 d following exposure to 10 (upper row) and 30 mg/m^3 (lower row) FSD 8. In this figure the responses to MCh are normalized in terms of the maximum contractile response obtained during the addition of MCh to the IL bath. Refer to the legend of Fig. 14 for *n* values. *$P < 0.05$, air-breathing controls *vs.* FSD 8-exposed.

panel. It was readily apparent that the NHBEs were also polarized with respect to cytokine release into the media. The changes in cytokine levels induced by FSD 8 (Figs. 22 and S11) were, for the most part, not robust, in line with the lack of elevation in LDH levels. The occurrence of significant changes was observed in most cases at 0.1 and 1 mg/well, in both the apical and basolateral media. Changes at higher doses were observed in EGF, ENA-78, eotaxin-2, FGF-2, fractalkine, GM-CSF, IL-1β, IL-4, IP-10, MDC, PDGF-AA, PDGF-BB, RANTES, TARC, TRAIL, and VEGF-A in both the apical and basolateral media. Alterations to TGF-α, and eotaxin-1 occurred only in the apical medium, whereas changes in G-CSF, IL12P40, and IL-12P70 only occurred in the basolateral medium. There were some significant changes in both apical and basolateral media at the lower doses of FSD 8 (0.0001, 0.001, and 0.01 mg/well), although these changes were far less frequent. These changes occurred apically in EGF, eotaxin-2, GM-CSF, and IL-1RA. Changes in basolateral medium at lower doses of FSD 8 occurred in EGF, GM-CSF, IL-18, IL-1RA, and TNF-β. The regression trends of the significant cytokine/chemokine changes are presented in Fig. 22.

4. Discussion

Little is currently known about the health effects of respirable FSD exposures that result from working at hydraulic fracturing sites. As quartz is the main component of the sands used in fracking, silicosis, such as that acquired by breathing silica dust in other occupations, is a potential outcome (Esswein et al., 2013; Quail, 2017). Silicosis is a well-documented risk to workers in a variety of industries using dusts containing crystalline silica. The major, but not the only determinant of silicosis risk from silica containing dusts, is the silica composition and the exposure level (National Institute for Occupational Safety and Health, 2002). FSD 8 is predominantly α-quartz, and differs from pure crystalline silica, *i.e.*, MIN-U-SIL, in its mineralogical composition (Fedan et al., 2020). This study did not evaluate the risk of chronic silicosis. Instead, it evaluated functional and potentially early endpoint effects of FSD 8 in a short-term rat inhalation study with a post-exposure recovery period.

This study was designed such that for both exposure concentrations of FSD 8, *i.e.*, 10 or 30 mg/m^3, the experimental post-exposure time points of 1, 7, 27, and 90 d would span the typical window for development of the pathophysiological and functional changes associated previously with the effects of MIN-U-SIL in a rat model (Castranova et al., 2002; Porter et al., 2004). However, the investigation was not intended as a side-by-side comparison of MIN-U-SIL *vs.* FSD 8 effects in every biological respect; a bulk of the experiments reported here have never been done following inhalation of MIN-U-SIL in rats. Nevertheless, there is some basis for some comparisons between the effects of MIN-U-SIL and FSD 8. The first, and surprising, sign that FSD 8 does not behave in a similar manner to crystalline silica, was the clearance rate of FSD 8 from the lungs. After sub-chronic exposures of rats, MIN-U-SIL has a very long retention time in the lungs, *i.e.*, a lung clearance half-life of ~82 d based on the 20 d-exposure to 15 mg/m^3 MIN-U-SIL with a 32-d clearance post-exposure measurement period (Porter et al., 2004). The ~82-d half-life for MIN-U-SIL is, therefore, substantially longer than the 11.3-d half-life of FSD 8, as determined by enhanced dark-field microscopy in this study. Examination of lung sections from FSD 8-exposed animals indicated that by 90 d post-exposure, the percentage of FSD 8 remaining in the lungs was only 0.1%. The fact that clearance of the FSD 8 was nearly complete by 90 d establishes a potentially important difference in the biological handling of FSD 8 compared to pure crystalline silica. A caveat that must be investigated, however, is to determine whether the

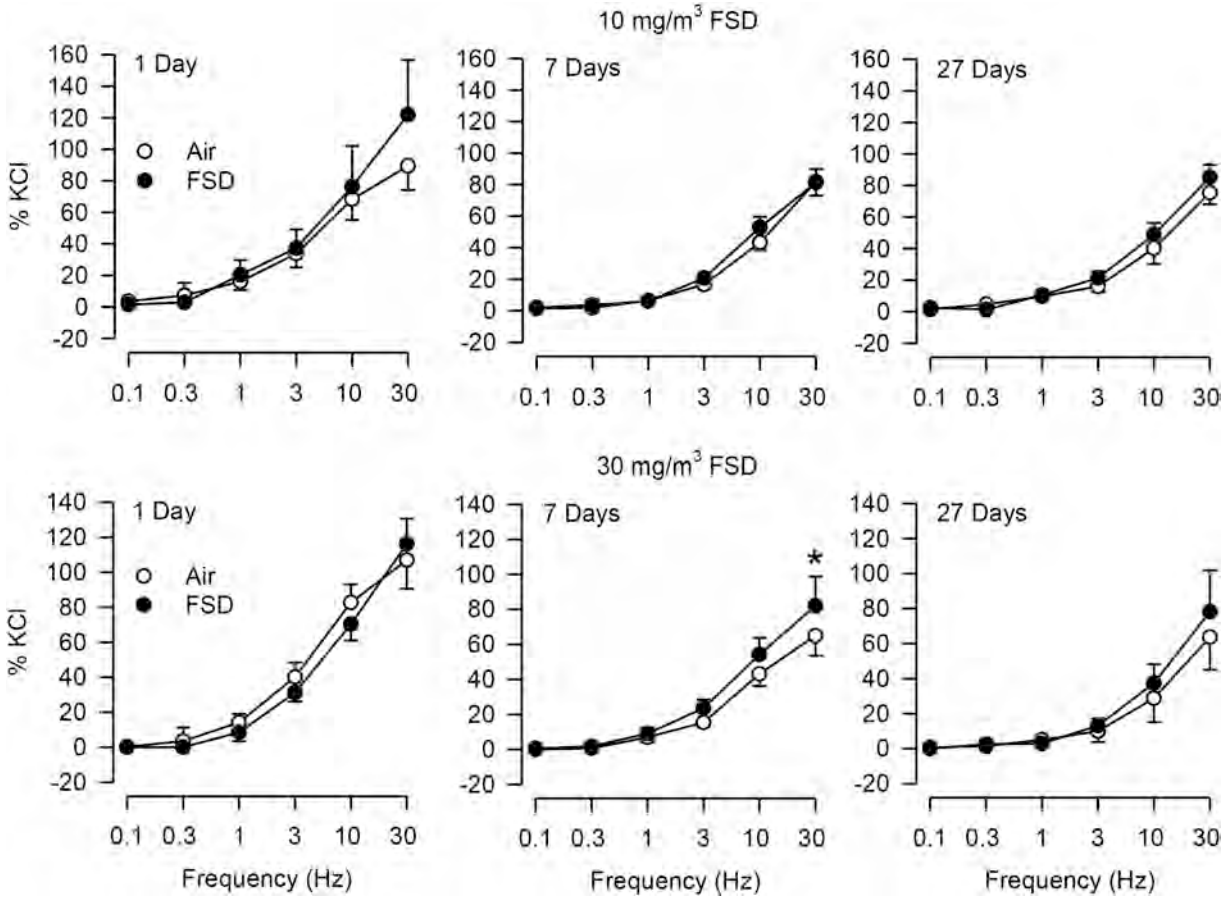

Fig. 16. Frequency-response curves from tracheal strips 1, 7 and 27 d following inhalation of 10 mg/m^3 FSD 8 (upper row or panels) or 30 mg/m^3 FSD 8 (lower row of panels). $n = 8$ per group per time point except for 10 mg/m^3 FSD 8 at 7 d post-exposure for which $n = 7$. *$P < 0.05$, air-breathing controls *vs.* FSD 8-exposed.

clearance half-life of MIN-U-SIL reported earlier was influenced by the greater number of days of exposure and post-exposure, and lung burden, inasmuch as its longer half-life was assessed from experiments in which animals were exposed to MIN-U-SIL for longer periods.

A second difference between the effects of FSD 8 and MIN-U-SIL was noted in lung weights. The lung weights of the FSD 8-exposed animals were not increased in comparison to the control lungs removed from air-breathing animals. In previous studies with MIN-U-SIL, the lung weights were increased both immediately after the end of the exposures as well as after the recovery period (Porter et al., 2004). This is possibly a reflection of the rapid clearance of FSD 8 from the lungs compared to MIN-U-SIL.

LDH release into the BAL fluid by damaged cells is a consistent component of the progression toward pulmonary inflammation in MIN-U-SIL-exposed rats (Castranova et al., 2002; Porter et al., 2004). Evidence for this effect was sought in the present investigation by examining whether FSD 8 treatment could evoke LDH release *in vitro*. In the preceding report (Fedan et al., 2020), i.t. instillation with nine FSDs did not evoke LDH release, whereas MIN-U-SIL did. In this study, exposure of cultured NHBE cells to FSD 8 did not result in LDH release from NHBEs. (It is of interest that LDH release was polarized across the epithelium, being greater from the apical surface than from the basolateral surface of the cells.) This finding also agrees with evidence obtained in the companion paper (Sager et al., 2020), in which it was observed that LDH levels in the BAL of rats were not elevated after FSD 8 inhalation exposure. Taken together, the lack of LDH release into the BAL fluid or from NHBE cells *in vitro* is another indicator that FSD 8 is less bioactive than MIN-U-SIL from the standpoint of being able to stimulate an inflammatory response in the lung.

FSD 8 evoked release of cytokines and chemokines from cultured primary NHBE cells into apical and basolateral media. (It is, again, of interest that cytokine release into the media also was polarized across the epithelium.) Regression analysis of chemokine/cytokine levels *vs.* FSD 8 doses eliciting significant changes was performed to determine if the dose-related trends were increasing or decreasing. Overall, the magnitudes of change of the mediators were moderate, in line with the mild inflammation observed in the lung (Sager et al., 2020). Of note was the increase in platelet derived growth factor-AA (PDGF-AA). Epithelial cells increase production of PDGF-AA when they are exposed to mineral dusts that result in fibrosis and silicosis; thus, PDGF-AA is considered an intermediary in the mechanism leading to silicosis (Dai et al., 1998; Mossman and Churg, 1998; Wang et al., 2017). In this study, the regression analysis for PDGF-AA revealed a decrease in release with increasing FSD 8 concentration apically, but a trend for increase in the basolateral medium. This suggests that NHBE cell signals favored inflammatory and fibrogenic responses to FSD 8 *in vitro*. Additionally, a similar trend (apical decrease and basolateral increase) was apparent for vascular endothelial growth factor-A (VEGF-A), which signals through the VEGF receptor 1 (VEGFR1). VEGFR1 signaling is necessary for monocyte migration (Claesson-Welsh, 2016). This suggests that the NHBE cells were signaling for an inflammatory response to FSD 8. Trends for increases in the levels of TGF-α, and IL-1β, which also have been implicated in the progression of fibrosis after crystalline silica exposure (Castranova et al., 2002; Kawasaki, 2015; Pollard, 2016), occurred in response to treatment with FSD 8. These findings suggest that FSD 8 caused a mild pro-inflammatory/fibrogenic signal in lung

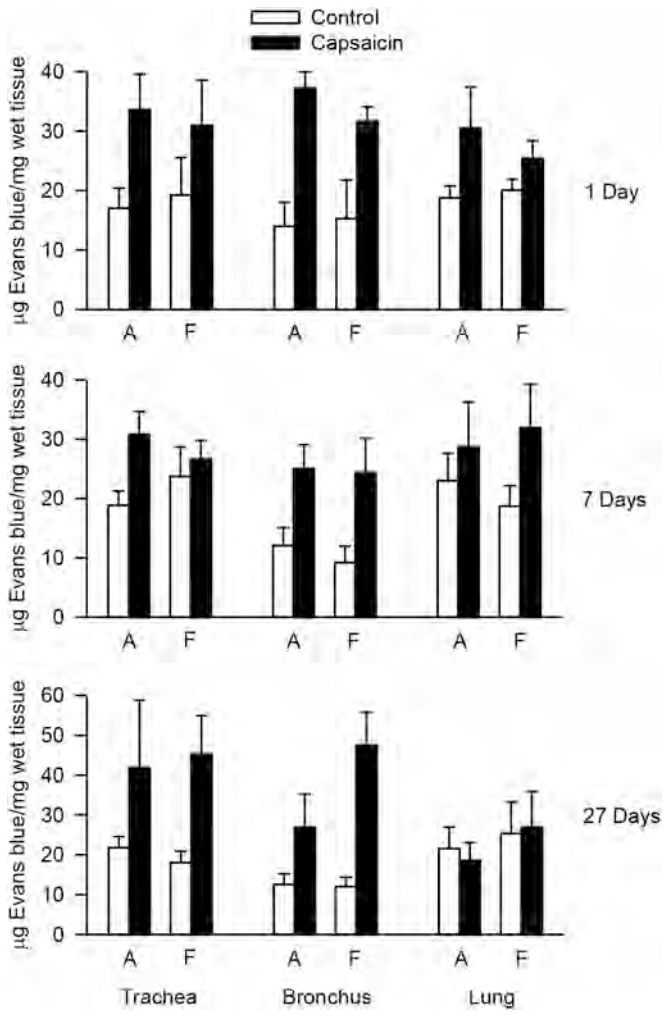

Fig. 17. Effect of inhalation of 30 mg/m^3 FSD 8 on Evans blue dye extravasation in trachea, bronchi and lung in response to capsaicin, 1, 7 and 27 d after exposure. A, air-breathing controls; F, FSD 8-exposed animals. $n = 6$ for all groups and time points except air + capsaicin day 1 post-exposure and FSD 8 no capsaicin day 27 post-exposure, for which $n = 5$. (For interpretation of the references to colour in this figure legend, the reader is referred to the web version of this article.)

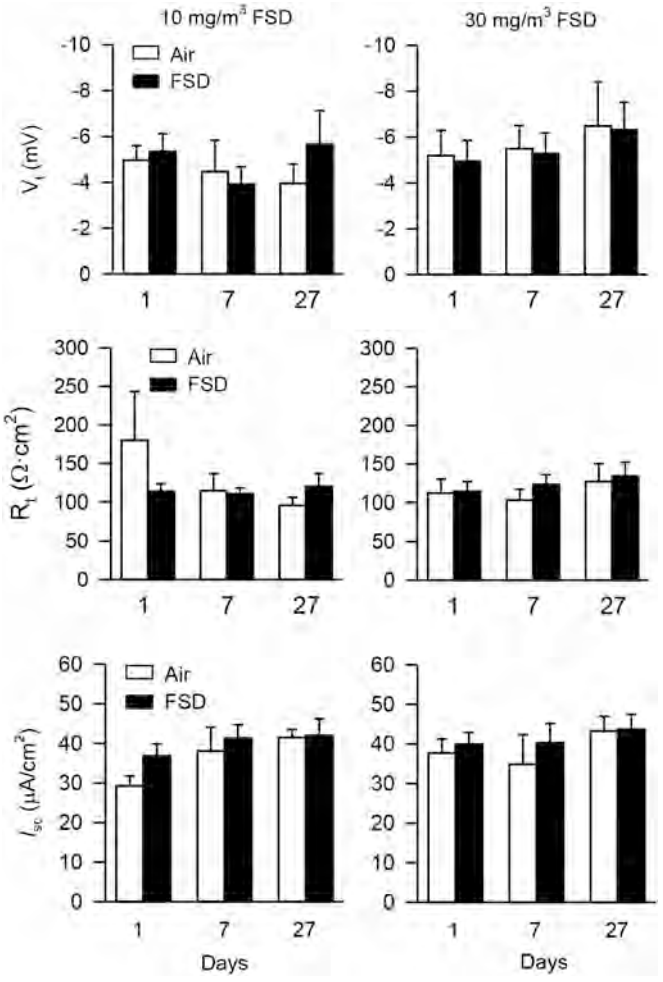

Fig. 18. Basal V_t, R_t and I_{sc} values of tracheal epithelium from animals exposed to 10 mg/m^3 FSD 8 (left column) or 30 mg/m^3 FSD 8 (right column) or filtered air at 1, 7 and 27 d after exposure. n values were as follows: for 10 mg/m^3, contol, $n = 8$, 8 and 5, and FSD 8, $n = 8$, 7, and 6, respectively, for 1, 7 and 27 d post-exposure periods; for 30 mg/m^3, control, $n = 8$, 8 and 8, and FSD 8, $n = 8$, 7, and 8, respectively, for 1, 7 and 27 d post-exposure periods.

epithelial cells *in vitro*. Were this to occur in epithelial cells *in vivo*, the magnitude of the signal is likely to be smaller than that triggered by MIN-U-SIL and more easily homeostatically managed. In fact, Sager et al. (2020) observed that inhaled FSD 8 did not significantly affect cytokine levels in BAL fluid.

To re-iterate, many of the experiments described in this study have not been performed using MIN-U-SIL and there is, therefore, no basis for comparing previous findings to ascertain how closely the effects of MIN-U-SIL and FSD 8 resemble each other in every respect. The potential contribution of these changes to the development of silicosis is undefined. For example, no change in basal lung mechanics in response to FSD 8 inhalation was observed; however, in response to 10 mg/m^3 FSD 8 exposure, the MCh dose-response curves for C_{dyn} responses was shifted to the left at 7 d post-exposure. Additionally, in response to 30 mg/m^3 FSD 8 exposure, the MCh dose-response curves for R_L responses shifted to the left at 7 d post-exposure. These changes resolved by 27 d post-exposure. Thus, under certain conditions, airway hyperreactivity to MCh was induced *in vivo*. With present data we cannot elucidate mechanisms for the changes in reactivity to MCh as being a manifestation of an allergic or asthmatic response, based on results obtained in other papers in this series. Levels of endotoxin in FSDs (Fedan et al., 2020) were found to be below a level that would produce an inflammatory effect. Sager et al. (2020) observed that FSD 8 inhalation did not produce inflammation in the lung. We cannot eliminate the possibility that other, unidentified biological agents are present in the FSD 8, and have no insight at present about their potential etiological role in affecting reactivity to MCh.

Likewise, changes in smooth muscle reactivity to MCh *in vitro* were also observed. The 10 mg/m^3 FSD 8-exposed animals exhibited reduced reactivity to MCh applied extraluminally, and increased reactivity to MCh intraluminally, at 7 d post-exposure, indicative of an effect of FSD 8 on airway smooth muscle, which suggests that epithelial barrier function or modulation of EpDRF were reduced. Interestingly, at 30 mg/m^3 FSD 8, there was a decrease in the IL maximum response to MCh relative to the EL maximum whereas, at 10 mg/m^3 FSD 8, there was an increase in the maximum response. All these changes were resolved by 27 d post-

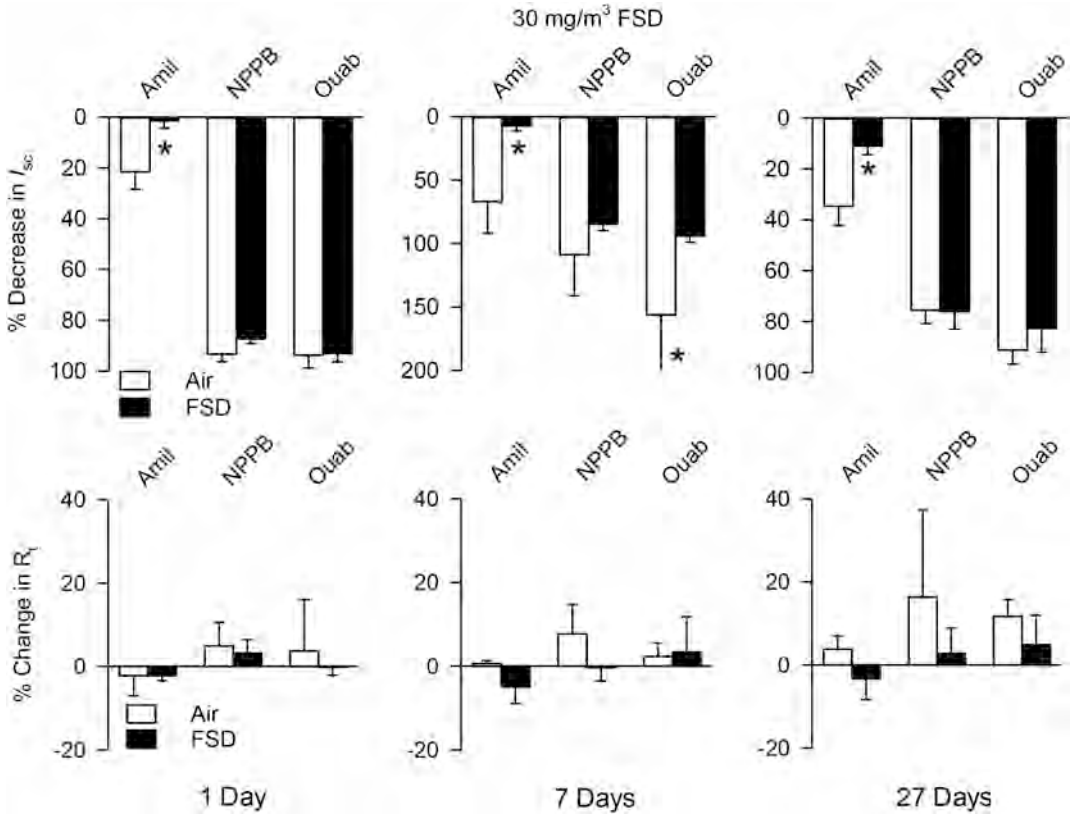

Fig. 19. Effect of inhalation of 30 mg/m^3 FSD 8 on responses of tracheal epithelium to ion transport inhibitors 1 day (left column), 7 d (middle column) and 27 d (right column) post-exposure. The Figure depicts the effects of FSD 8 exposure on bioelectric responses of the epithelium to amiloride added to the apical chamber, NPPB added to the apical chamber, and ouabain added to the basolateral chamber. The data are normalized with respect to basal values shown in Fig. 19, and are expressed in terms of responses as % change from basal values. Fig. S9 depicts the raw data from which the normalized data were derived. *n* values were as follows: for 10 mg/m^3, control, $n = 8$, 8 and 5, and FSD 8, $n = 8$, 7, and 6, respectively, for 1, 7 and 27 d post-exposure periods; for 30 mg/m^3, control, $n = 8$, 8 and 8, and FSD 8, $n = 8$, 7, and 8, respectively, for 1, 7 and 27 d post-exposure periods. *$P < 0.05$, air-breathing controls *vs.* FSD 8-exposed.

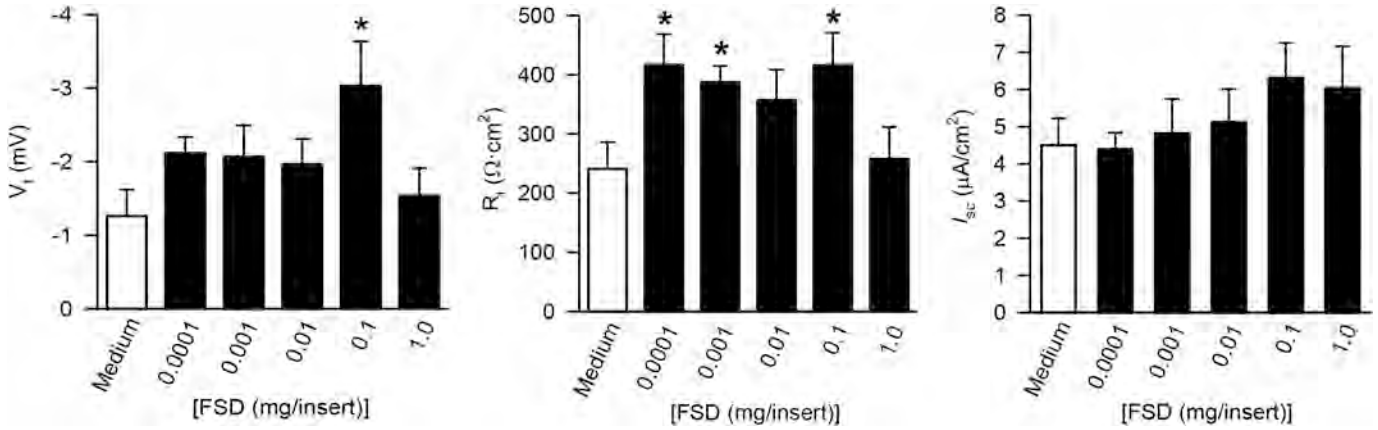

Fig. 20. Basal V_t, R_t and I_{sc} values of NHBE cells exposed to 0.0001, 0.001, 0.01, 0.1, and 1 mg/insert FSD 8 ($n = 8$). FSD 8 induced effects on V_t at 0.1 mg/insert and on R_t at 0.0001, 0.001, and 0.1 mg/insert. No changes were observed in I_{sc}. *$P < 0.05$, medium *vs.* FSD 8-exposed NHBE cells.

exposure. The basis for the qualitative changes in reactivity of the perfused trachea at different doses and times is difficult to explain, but they do indicate that FSD 8 can transiently affect reactivity *in vivo* and *in vitro*. Additionally, it appears that the release of acetylcholine from parasympathetic, post-ganglionic neurons and/or post-junctional muscarinic receptors was possibly affected by 30 mg/m^3 FSD 8 at 7 d post-exposure at 30 Hz. These changes indicate that inhaled FSD 8 can affect airway function in heretofore undescribed ways. The trend for

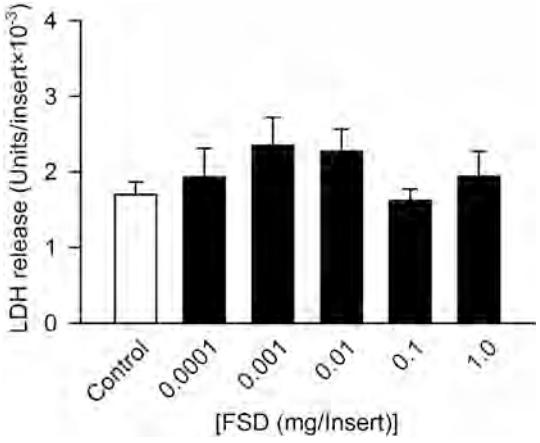

Fig. 21. Effect of FSD 8 on LDH release into the apical medium following an 18-h incubation of NHBE cells with FSD 8. There were no effects of FSD 8 on LDH release at any FSD 8 concentration. LDH was not released into the basolateral medium of control or FSD 8-exposed cells. $n = 8, 8, 8, 8, 7, 8$ for control, 0.0001, 0.001, 0.01, 0.1, and 1 mg/insert, respectively.

observed changes to resolve by 27 d post-exposure, regardless of the parameter measured, is another characteristic of FSD 8 that is not consistent with exposure to crystalline silica in the rat model in the context of progressive silicosis development. The resolution of these functional effects may be associated with the rapid clearance of FSD 8 from the lung, since we calculated an 11.3 d half-life in this study.

Finally, the last notable change after exposure to FSD 8 was with respect to ion transport in the trachea and primary NHBE cells. In tracheas from animals exposed to 30 mg/m^3 FSD 8, Na^+ transport across the epithelium was attenuated at 1, 7, and 27 d post-exposure. This was the only parameter measured in this study that remained affected for the duration of the study period. It is unknown whether Na^+ transport is affected in response to inhalation of crystalline silica. Additionally, at 7 d post-exposure, ouabain, an inhibitor of the Na^+, K^+-pump, had an attenuated effect on I_{sc}. Nevertheless, decrease in Na^+ absorption could result in hydration of the airway surface liquid, which could perturb fluid balance in the lung (Bartoszewski et al., 2017) and particle clearance. Changes in airway surface liquid have been linked to altered cilia function and changes to mucociliary clearance (Widdicombe and Widdicombe, 1995). Along similar lines, in NHBE cells, FSD 8 treatment resulted in elevation of baseline R_t values. The airway epithelium appears to be a site at which FSD 8 evokes long-lasting functional changes, even after most particles are cleared. Future studies will be needed to understand why FSD 8 inhalation exposure inhibited Na^+ transport while not affecting R_t in fresh tracheal preparations, whereas R_t but not Na^+ transport was altered in NHBE cells *in vitro*. The notion that FSD 8 could affect Na^+ channels is somewhat tenable, inasmuch as silica nanoparticles (albeit amorphous) inhibited transient receptor potential vanilloid 4 (TRPV4) channels in mouse cultured tracheal epithelial cells (Sanchez et al., 2017).

The elemental analyses of nine FSDs reported in the previous study (Fedan et al., 2020) revealed differences among the dusts and many bioactivity dissimilarities between the nine FSDs and MIN-U-SIL. In the present study, differences among bioactivities of FSD 8 and MIN-U-SIL also were revealed. Some effects of FSD 8 on ventilatory and non-ventilatory parameters were observed which appear to resolve in time during the post-exposure recovery period. A strong pro-inflammatory response to FSD 8, which is also typically associated with the effects of MIN-U-SIL, was not evident under the conditions of our experiments. The electrophysiology of airway epithelium was altered by exposure to FSD 8, the mechanisms of which need further exploration.

Growth Factors

Cytokine	Apical Trend	Basolateral Trend
TGF-α	↑	↑
TNFB	N/A	↑
EGF	↓	↓
FGF-2	↓	↓
PDGF-BB	↓	↓
TRAIL	↓	↓
G-CSF	N/A	↓

Inflammatory Mediators

Eotaxin-2	↑	↑
GM-CSF	↑	↑
IL-1β	↑	↑
IL-1RA	↑	↑
IL-4	↑	↑
ENA-78	↓	↓
Fractalkine	↓	↓
IP-10	↓	↓
MDC	↓	↓
PDGF-AA	↓	↑
RANTES	↓	↓
TARC	↓	↓
VEGF-A	↓	↑
IL-18	N/A	↓
IL-12P40	N/A	↓
IL-12P70	N/A	↓

Fig. 22. Effect of FSD 8 on cytokine presence in apical or basolateral medium following an 18-h incubation of NHBE cells with FSD 8. Linear regression was utilized to determine the trend as either increasing or decreasing across the concentrations of FSD 8 (control, 0.0001, 0.001, 0.01, 0.1, and 1 mg/insert FSD 8). $n = 3$ for all exposure groups.

Disclaimer

The findings and conclusions in this report are those of the authors and do not necessarily represent the official position of the National Institute for Occupational Safety and Health, Centers for Disease Control and Prevention. Mention of any company or product does not constitute endorsement by the National Institute for Occupational Safety and Health (NIOSH), Centers for Disease Control and Prevention (CDC).

Supplementary data to this article can be found online at https://doi.org/10.1016/j.taap.2020.115284.

Declaration of Competing Interest

The authors declare that they have no conflicts of interest in relation to this publication.

Acknowledgements

The authors are very grateful to Ann Hubbs for helpful discussions. Funding was provided by the National Institute for Occupational Safety and Health, Project Number 7927ZLDC.

References

Anderson, S.E., Shane, H., Long, C., Marrocco, A., Lukomska, E., Roberts, J.R., Marshall, N., Fedan, J.S., 2020. Biological effects of inhaled hydraulic fracturing sand dust. VIII. Immunotoxicity. Toxicol. Appl. Pharmacol. (Manuscript submitted to this journal as a tandem paper to accompany this manuscript.).

Bartoszewski, R., Matalon, S., Collawn, J.F., 2017. Ion channels of the lung and their role in disease pathogenesis. Am. J. Phys. Lung Cell. Mol. Phys. 313, L859–L872.

Castranova, V., Porter, D., Millecchia, L., Ma, J.Y., Hubbs, A.F., Teass, A., 2002. Effect of inhaled crystalline silica in a rat model: time course of pulmonary reactions. Mol. Cell. Biochem. 234-235, 177–184.

Claesson-Welsh, L., 2016. VEGF receptor signal transduction – a brief update. Vacs. Pharmacol. 86, 14–17.

Dai, J., Gilks, B., Price, K., Churg, A., 1998. Mineral dusts directly induce epithelial and interstitial fibrogenic mediators and matrix components in the airway wall. Am. J. Respir. Crit. Care Med. 158, 1907–1913.

Esswein, E.J., Breitenstein, M., Snawder, J., Kiefer, M., Sieber, W.K., 2013. Occupational exposures to respirable crystalline silica during hydraulic fracturing. J. Occup. Environ. Hyg. 10, 347–356.

Fedan, J.S., 2020. Biological effects of inhaled hydraulic fracturing sand dust. I. Scope of the investigation. Toxicol. Appl. Pharmacol. (Manuscript submitted to this journal as a tandem paper to accompany this manuscript.).

Fedan, J.S., Frazer, D.G., 1992. Influence of epithelium on the reactivity of guinea-pig isolated, perfused trachea to bronchoactive drugs. J. Pharmacol. Exp. Ther. 262, 741–750.

Fedan, J.S., Millecchia, L.L., Johnston, R.A., Rengasamy, A., Hubbs, A., Dey, R.D., Yuan, L.X., Watson, D., Goldsmith, W.T., Reynolds, J.S., Orsini, L., Dortch-Carnes, J., Cutler, D., Frazer, D.G., 2000. Effect of ozone treatment on airway reactivity and epithelium-derived relaxing factor in guinea pigs. J. Pharmacol. Exp. Ther. 293, 724–734.

Fedan, J.S., Van Scott, M.R., Johnston, R.A., 2001. Pharmacological techniques for the in vitro study of airways. J. Pharmacol. Toxicol. Methods 45, 159–174.

Fedan, J.S., Roberts, J.R., Barger, M., Snawder, J.E., Schwegler-Berry, D., Friend, S., Leonard, S.S., Thompson, J.A., Jackson, M.C., Dozier, A.K., Coyle, J., Kashon, M.L., Park, J.-H., McKinney, W., 2020. Biological effects of inhaled hydraulic fracturing sand dust. II. Inhalation exposure system, particle characterization, and effects following intratracheal instillation. Toxicol. Appl. Pharmacol. (Manuscript submitted to this journal as a tandem paper to accompany this manuscript.).

Hubbs, A., Greskevitch, M., Kuempel, E., Suarez, F., Toraason, M., 2005. Abrasive blasting agents: designing studies to evaluate relative risk. J. Toxicol. Environ. Health A 68, 999–1016.

ICRP, 1994. Human respiratory tract model for radiological protection: a report of a task group of the international commission on radiological protection. Ann ICRP 24 (1–3), 267–272.

Investigative Team, 2020. Biological effects of inhaled hydraulic fracturing sand dust. IX. Summary and significance. Toxicol. Appl. Pharmacol. (Manuscript submitted to this journal as a tandem paper to accompany this manuscript.).

Kawasaki, H., 2015. A mechanistic review of silica-induced inhalation toxicity. Inhal. Toxicol. 27, 363–377.

Krajnak, K., Russ, K.A., McKinney, W., Waugh, S., Zheng, W., Kan, H., Kashon, M.L., Johnson, C., Cumpston, J., Fedan, J.S., 2020. Biological effects of inhaled hydraulic fracturing sand dust. IV. Exposure to fracking sand dust results in changes in factors associated with cardiovascular dysfunction. Toxicol. Appl. Pharmacol. (Manuscript submitted to this journal as a tandem paper to accompany this manuscript.).

Kuempel, E.D., Tran, C.-L., Bailer, A.J., Porter, D.W., Hubbs, A.F., Castranova, V., 2001. Biological and statistical approaches to predicting human lung cancer risk from silica. J. Environ. Pathol. Toxicol. Oncol. 20 (Suppl. 1), 15–32.

Ma, J., Mercer, R.R., Barger, M., Schwegler-Berry, D., Cohen, J.M., Demokritou, P., Castranova, V., 2015. Effects of amorphous silica coating on cerium oxide nanoparticles induced pulmonary responses. Toxicol. Appl. Pharmacol. 288, 63–73.

McKinney, W., Jackson, M., Sager, T.M., Reynolds, J.S., Chen, B.T., Afshari, A., Krajnak, K., Waugh, S., Johnson, C., Mercer, R.R., Frazer, D.G., Thomas, T.A., Castranova, V., 2012. Pulmonary and cardiovascular responses of rats to inhalation of a commercial antimicrobial spray containing titanium dioxide nanoparticles. Inhal. Toxicol. 24, 447–457.

Mercer, R.R., Russell, M.L., Crapo, J.D., 1991. Radon dosimetry based on the depth distribution of nuclei in human and rat lungs. Health Phys. 61, 117–130.

Mercer, R.R., Russell, M.L., Roggli, V.L., Crapo, J.D., 1994. Cell number and distribution in human and rat airways. Am. J. Respir. Cell Mol. Biol. 10, 613–624.

Mercer, R.R., Scabilloni, J.F., Hubbs, A.F., Wang, L., Battelli, L.A., McKinney, W., Castranova, V., Porter, D.W., 2013. Extrapulmonary transport of MWCNT following inhalation exposure. Part Fibre Toxicol 10, 38.

Mercer, R.R., Scabilloni, J.F., Wang, L., Battelli, L.A., Antonini, J.M., Roberts, J.R., Qian, Y., Sisler, J.D., Castranova, V., Porter, D.W., Hubbs, A.F., 2018. The fate of inhaled nanoparticles: detection and measurement by enhanced dark-field microscopy. Toxicol. Pathol. 46, 28–46.

Mossman, B.T., Churg, A., 1998. Mechanisms in the pathogenesis of asbestosis and silicosis. Am. J. Respir. Crit. Care Med. 157, 1666–1680.

MPPD, 2010. Multiple-path Particle Dosimetry Model, Version 2.11. Applied Research Associates, Inc.. Albuquerque, NM, pp. 2010.

National Institute for Occupational Safety and Health, 2002. Health Hazard Review. Health effects of occupational exposure to respirable crystalline silica.

Olgun, N.S., Morris, A.M., Stefaniak, A.B., Bowers, L.N., Knepp, A.K., Duling, M.G., Mercer, R.R., Kashon, M.L., Fedan, J.S., Leonard, S.S., 2020. Biological effects of inhaled hydraulic fracturing sand dust. III. Cytotoxicity and pro-inflammatory responses caused in murine cultured macrophage cells. Toxicol. Appl. Pharmacol. (Manuscript submitted to this journal as a tandem paper to accompany this manuscript.).

Pollard, K.M., 2016. Silica, silicosis, and autoimmunity. Front. Immunol. 7, 97.

Porter, D.W., Hubbs, A.F., Mercer, R., Robinson, V.A., Ramsey, D., McLaurin, J., Khan, A., Battelli, L., Brumbaugh, K., Teass, A., Castranova, V., 2004. Progression of lung inflammation and damage in rats after cessation of silica inhalation. Toxicol. Sci. 79, 370–380.

Quail, M.T., 2017. Overview of silica-related clusters in the United States: will fracking operations become the next cluster? J. Environ. Health 79, 20–27.

Raabe, O.G., Al-Bayati, M.A., Teague, S.V., Rasolt, A., 1988. Regional deposition of inhaled monodisperse coarse and fine aerosol particles in small laboratory animals. Ann. Occup. Hyg. 32, 53–63.

Sager, T.M., Roberts, J.R., Umbright, C.M., Barger, M., Kashon, M.L., Fedan, J.S., Joseph, P., 2020. Biological effects of inhaled hydraulic fracturing sand dust. V. Pulmonary inflammatory, cytotoxic and oxidant effects. Toxicol. Appl. Pharmacol. (Manuscript submitted to this journal as a tandem paper to accompany this manuscript.).

Sanchez, A., Alvarez, J.L., Demydenko, K., Jung, C., Alpizar, Y.A., Alvarez-Collazo, J., Cokic, S.M., Valverde, M.A., Hoet, P.H., Talavera, K., 2017. Silica nanoparticles inhibit the cation channel TRPV4 in airway epithelial cells. Part. Fibre Toxicol. 14, 43.

Sriram, K., Lin, G.X., Jefferson, A.M., McKinney, W., Jackson, M.C., Cumpston, A., Cumpston, J.L., Cumpston, J.B., Leonard, H.D., Kashon, M.L., Fedan, J.S., 2020. Biological effects of inhaled hydraulic fracturing sand dust. VII. Neuroinflammation and altered synaptic protein expression. Toxicol. Appl. Pharmacol. (Manuscript submitted to this journal as a tandem paper to accompany this manuscript.).

Stone, K.C., Mercer, R.R., Gehr, P., Stockstill, B., Crapo, J.D., 1992. Allometric relationships of cell numbers and size in the mammalian lung. Am. J. Respir. Cell. Mol. Biol. 6, 235–243.

Wang, X., Sun, B., Liu, S., Xia, T., 2017. Structure activity relationships of engineered nanomaterials in inducing NLRP3 inflammasome activation and chronic lung fibrosis. NanoImpact 6, 99–108.

Widdicombe, J.H., Widdicombe, J.G., 1995. Regulation of human airway surface liquid. Respir. Physiol. 99, 3–12.